JOTCS B
Journal of the Turkish Chemical Society
Section: B
Chemical Engineering

TURKISH CHEMICAL SOCIETY

The Investigation of Oven and Vacuum Oven Drying Kinetics and Mathematical Modeling of Golden Berries[1]

Ekin Kıpçak[1*]

[1]Yıldız Technical University, Faculty of Chemical and Metallurgical Engineering, Department of Chemical Engineering, İstanbul, 34210, Turkey

Abstract: Golden berry (*Physalis peruviana*) is a fruit that is natively cultivated in the Andean region. Due to its significant nutritional and functional properties, golden berry has been gradually attracting worldwide attention. In this study, oven and vacuum oven drying of golden berries were performed at 60, 70 and 80 °C. Throughout the experiments, the drying kinetic parameters of effective moisture diffusivity (D_{eff}) and activation energy (E_a) were investigated. Moreover, mathematical modeling of drying data was established with the most known modeling equations presented in literature. Experiments revealed that the drying times decreased with increasing temperature and with vacuum addition. The highest and lowest drying times were encountered as 480 minutes in oven drying at 60 °C, and 195 minutes in vacuum oven drying at 80 °C, respectively. D_{eff} values were calculated between 1.95×10^{-10}-3.80×10^{-10} m^2/s and 2.20×10^{-10}-5.45×10^{-10} m^2/s for oven and vacuum oven drying, respectively. E_a values, on the other hand, were found as 32.81 kJ/mol for oven drying and 44.30 kJ/mol for vacuum oven drying. Among the fourteen mathematical models applied to drying curve data, Midilli & Kucuk model provided the best fit for both oven and vacuum oven drying.

Keywords: Drying Kinetics, Golden Berry, Mathematical Modeling, Oven Drying, Vacuum Oven Drying.

Submitted: October 16, 2022. **Accepted:** December 22, 2022.

Cite this: Kıpçak, E. (2023). The Investigation of Oven and Vacuum Oven Drying Kinetics and Mathematical Modeling of Golden Berries. Journal of the Turkish Chemical Society, Section B: Chemical Engineering, 6(1), 1–8.

***Corresponding author. E-mail:** eyildir@yildiz.edu.tr.

1. INTRODUCTION

Golden berry (*Physalis peruviana*), also called cape gooseberry, is an exotic fruit that is natively cultivated in the Andean region of the world (Etzbach et al., 2020; Junqueira et al., 2017). It is covered by a yellow peel and is protected through a surrounding dry parchment-like husk, named as calyx, which serves as a protective shield against adverse climatic conditions, birds, and insects (Bravo & Osorio, 2016; Lopez et al., 2013; Nawirska-Olszańska et al., 2017). It is a functional food that attracts particular attention due its nutritional composition and content of bioactive components. Golden berries contain substantial amount of vitamins (especially Vitamins A, C, K, and B complexes), minerals, fibers, ascorbic acid, polyphenols and carotenoids (Bravo & Osorio, 2016; Junqueira et al., 2017; Lopez et al., 2013; Nawirska-Olszańska et al., 2017; Puente et al., 2021). It is widely used in the field of medicine for the remedy of various diseases, due to its anti-parasitic, anti-infectious, and diuretic properties (Bravo & Osorio, 2016). It was reported that golden berries are used in the treatment of cancer, hypertension, asthma, ulcer, hepatitis, dermatitis, malaria, and rheumatism (Karacabey, 2016; Ramadan, 2011). The high levels of Vitamin K, which is responsible for protein synthesis in charge of blood clotting and bone metabolism, reduce the risk of cardiac diseases and occurrence of cancer (Ramadan, 2011). Due to its fructose content, golden berry is also recommended for diabetics (Nawirska-Olszańska et al., 2017; Ramadan, 2011).

Considering all of the aforementioned desirable nutritional and functional properties, golden berry is

1 This paper was orally presented at the 1st IKSTC on 1-3 September 2022, Cankiri, Turkey.

gradually becoming a fruit of particular interest to the food industry. Nevertheless, golden berry is a rapidly perishable fruit, a property of which hinders its desired commercialization. Consequently, this phenomenon necessitates the investigation of efficient methods for the extensive preservation of golden berries. One of these preservation methods is drying. The main objective of food drying is to preserve foods and to increase their shelf lives, by decreasing their moisture contents in order to inhibit the activities of microorganisms. Moreover, transport and storage costs are reduced, since the use of refrigeration systems is not necessary. There are many conventional methods employed for the drying of fruits; however among these methods, oven drying offers the easiest and simplest and application. Furthermore, it provides a more homogeneous, hygienic, and rapid drying than the other conventional methods. In some studies, oven drying is assisted with the use of vacuum. Vacuum assistance protects fruits against oxidation, while simultaneously preserving their nutritional values, texture, taste, and color (Calín-Sánchez et al., 2014; Guiné, 2018; Kaleta & Górnicki, 2010; Pan et al., 2008).

In this study, oven and vacuum oven drying of golden berries were investigated. Although there are numerous articles in the literature regarding the antioxidant properties of golden berries, investigation on their drying characteristics is still very scarce. This being the motivation of the present research, golden berry drying experiments were performed at 60, 70, and 80 °C. Moreover, drying kinetic parameters including the effective moisture diffusivities and activation energies were calculated. Fourteen mathematical models present in the literature were applied to the drying curve data. The results obtained for drying with and without the assistance of vacuum were comparatively evaluated.

2. MATERIALS AND METHODS

2.1. Sample Preparation

Golden berries used in the experiments, cultivated in Mersin province of Turkey, were bought from a local supermarket in İstanbul, on October 2021. Similar sized golden berries were selected for the experiments with approximate radii of 2 cm. Before the experiments, the golden berries were horizontally divided into two pieces for the investigation of thin layer diffusion process. In each experiment, 10 g of golden berry samples were used, which were equivalent to two or three golden berries for each run. Prior to drying, the initial moisture content of the golden berries was determined by AOAC method (AOAC International, 1975), using a KH-45 hot air drying oven (Kenton, Guangzhou, China) at 105 °C for 2 hours. In this regard, the initial moisture content of the golden berries was determined as 74.93% on wet basis, and 2.989 kg of water/kg dry matter.

2.2. Drying Methods

In this study, two different drying methods were used for the drying of golden berries, which were oven drying and vacuum oven drying. In oven drying, Nüve EV-018 model oven (Nüve, Ankara, Turkey) was used. In vacuum-oven drying, on the other hand, the same oven was used with KNF N022AN.18 model vacuum pump (KNF, Freiburg, Germany). The pressure inside the oven was measured as 0.3 atm during the experiments. In order to calculate the kinetic parameters, the experiments were performed at three different temperatures that were 60, 70, and 80 °C. During the drying process, the golden berries were weighed by a Radwag AS 220.R2 digital balance (Radwag, Radom, Poland) in every 15 minutes. When the weights of the golden berries were reduced to approximately 5% of the moisture content, the drying process was stopped.

2.3. Drying Kinetics

In order to calculate the kinetic parameters, the moisture content (M) as kg water/kg dry matter, the drying rate (DR) as kg water/(kg dry matter×min) and the moisture ratio (MR) as dimensionless were calculated by using Equations (1), (2) and (3), respectively (Başlar et al., 2014; Doymaz et al., 2016; Ismail & Kocabay, 2018):

$$M = \frac{m_w}{m_d} \quad \text{(Eq. 1)}$$

$$DR = \frac{M_{t+dt} - M_t}{dt} \quad \text{(Eq. 2)}$$

$$MR = \frac{M_t - M_e}{M_0 - M_e} \quad \text{(Eq. 3)}$$

In the aforementioned equations, m_w represents the water content of the golden berries in kg, m_d is their dry matter content in kg, t is the drying time in minutes and M_{t+dt} is the amount of moisture during the time t+dt in kg water/kg dry matter. M_0, M_t and M_e represent the amount of initial moisture, moisture at any time t and moisture at equilibrium, respectively. Since the moisture levels at equilibrium are very low compared to the initial and instantaneous moisture values, M_e is neglected in the calculations (Amiri Chayjan & Shadidi, 2014; Calín-Sánchez et al., 2014).

To describe moisture diffusion in food drying, which usually occurs during the falling rate period, Fick's second law of diffusion is used (Crank, 1975). In the

present study, in order to perform the analytical solution of this equation, several assumptions were made, which are presented as follows:

• The shrinkage of the golden berries was neglected,
• The diffusion coefficient was accepted as constant,
• The mass transfer was assumed to occur symmetrically with respect to the center, only by diffusion.

Taking into account the foresaid assumptions, the analytical solution of Fick's second law for a thin layer with a thickness of 2 L is calculated with respect to Equation (4):

$$MR = \frac{8}{\pi^2}\sum_{n=1}^{\infty}\frac{1}{(2n+1)^2}\exp\left(\frac{-(2n+1)^2\pi^2 D_{eff}\times t}{4L^2}\right) \quad \text{(Eq. 4)}$$

In Equation (4) n is a positive integer, D_{eff} is the effective moisture diffusivity in m^2/s, t is the time in seconds and L is the half of the sample thickness in meters. For elongated drying times, n is assumed as 1 (Doymaz et al., 2016; Ismail & Kocabay, 2018). Thus, Equation (4) can be simplified to Equation (5) as presented below:

$$\ln(MR) = \ln\left(\frac{8}{\pi^2}\right) - \left(\pi^2\frac{D_{eff}\times t}{4L^2}\right) \quad \text{(Eq. 5)}$$

By using Equation (5), D_{eff} can be calculated from the slope of ln(MR) versus t plot. Once D_{eff} is calculated, its relation with temperature can be expressed by Arrhenius equation, which is presented in Equation (6) (19):

$$D_{eff} = D_o\exp\left(\frac{-E_a}{R(T+273.15)}\right) \quad \text{(Eq. 6)}$$

In the aforementioned equation D_0 is the pre-exponential factor in m^2/s, E_a is the activation energy in kJ/mol, R is the universal gas constant in kJ/(mol×K) and T is the drying temperature in °C. The activation energy, E_a, can be calculated from the slope of ln(D_{eff}) versus 1/T plot.

2.4. Mathematical Modeling of the Drying Process

For the mathematical modeling of the drying of golden berries, fourteen abundantly used mathematical models present in the literature were investigated. These mathematical drying models applied to the experimental data were Aghbaslo et al., Alibas, Henderson & Pabis, Jena et al., Lewis, Logarithmic, Midilli & Kucuk, Page, Parabolic, Peleg, Two-Term Exponential, Verma et al., Wang & Singh and Weibull models, which are presented in Table 1. For the models presented in Table 1, a, b, c, and g are coefficients; n is the drying exponent specific to each equation; k, k_1 and k_2 are drying coefficients and t is the time in minutes (Ismail & Kocabay, 2018; Kipcak et al., 2021; Ozyalcin & Kipcak, 2020, 2020).

Table 1: The mathematical drying models applied to the experimental data for oven drying and vacuum oven drying of golden berries.

Model Name	Parameter
Aghbashlo et al.	$MR = \exp(-k_1t/(1 + k_2t))$
Alibas	$MR = a\cdot\exp((-kt^n) + bt) + g$
Henderson & Pabis	$MR = a\cdot\exp(-kt)$
Jena et al.	$MR = a\cdot\exp(-kt + b\boxtimes t) + c$
Lewis	$MR = \exp(-kt)$
Logarithmic	$MR = a\cdot\exp(-kt) + c$
Midilli & Kucuk	$MR = a\cdot\exp(-kt^n) + bt$
Page	$MR = \exp(-kt^n)$
Parabolic	$MR = a + bt + ct^2$
Peleg	$MR = a + t/(k_1 + k_2t)$
Two-Term Exponential	$MR = a\cdot\exp(-kt) + (1 - a)\cdot\exp(-kat)$
Verma et al.	$MR = a\cdot\exp(-kt) + (1 - a)\cdot\exp(-gt)$
Wang & Singh	$MR = 1 + at + bt^2$
Weibull	$MR = a - b\cdot\exp(-(kt^n))$

In the modelling process, Statistica 6.0 software (Statsoft Inc., Tulsa, OK) was used for the nonlinear regressions based on Levenberg-Marquardt procedure and parameters. While using the program, the experimental data is entered and nonlinear regression is selected. Once the selected mathematical model is defined, the program used iterative algorithms to find the best fits for the unknown constants through the reductions in the sum of the squared errors. During the testing of the mathematical models, the coefficient of determination (R^2), reduced chi-square (χ^2) and root mean square error (RMSE) were calculated for the experimental and predicted MR values, the formulas of which are given in various studies in literature (Alibas, 2014; Uribe et al., 2022; Vega-Gálvez et al.,

2014; Zhu, 2018). The best model to describe the drying of golden berries was selected as the model giving the highest R^2, lowest χ^2 and lowest RMSE values (9).

3. RESULTS AND DISCUSSION

3.1. The Drying and Drying Rate Curves

Figure 1 and Figure 2 present the drying curves and the drying rate curves of oven drying and vacuum oven drying of golden berries, respectively. Considering Figure 1 first, it is seen that the drying times and the final moisture contents decreased with increasing temperature. Moreover, the drying times were observed to be shorter for vacuum oven drying. Similar results were obtained in literature studies (Ozyalcin & Kipcak, 2020). During the experiments made with oven drying, the drying times were found as 285, 300 and 480 minutes for drying temperatures of 80, 70, and 60 °C, respectively. On the other hand, these times reduced to 195, 285, and 435 minutes for the same drying temperatures during vacuum oven drying. From the moisture content point of view, vacuum oven drying yielded similar results. The initial moisture content of the golden berry samples, which was 2.989 kg water/kg dry matter, reduced to 0.156, 0.208, and 0.291 kg water/kg dry matter for oven drying at 80, 70, and 60 °C, respectively. For vacuum oven drying, the final moisture contents were calculated as 0.154, 0.204, and 0.269 kg water/kg dry matter for the same drying temperatures.

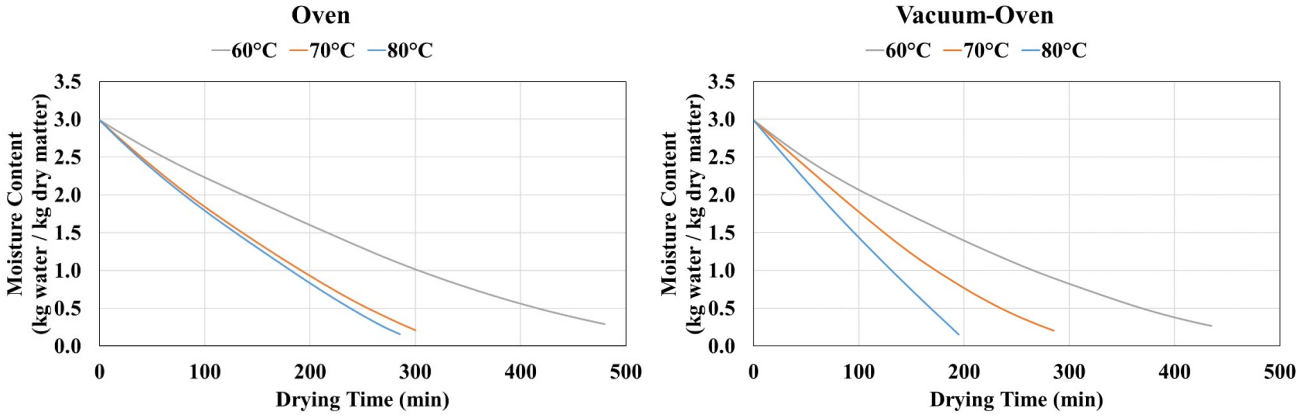

Figure 1: The oven and vacuum oven drying curves of golden berries.

For both of the drying methods, the rising-rate periods and falling-rate periods were observed as seen from Figure 2. In oven drying, the rising rate periods were obtained from the initial moisture content of 2.989 kg water/kg dry matter to 2.782, 2.798 and 2.861 kg water/kg dry matter for the drying temperatures of 80, 70,. and 60 °C, respectively. Then the falling-rate periods were encountered until the final moisture contents. For vacuum oven drying, the rising rate periods were obtained again from the initial moisture content of 2.989 kg water/kg dry matter to 2.744, 2.799, and 2.827 kg water/kg dry matter for the drying temperatures of 80, 70, and 60 °C, respectively.

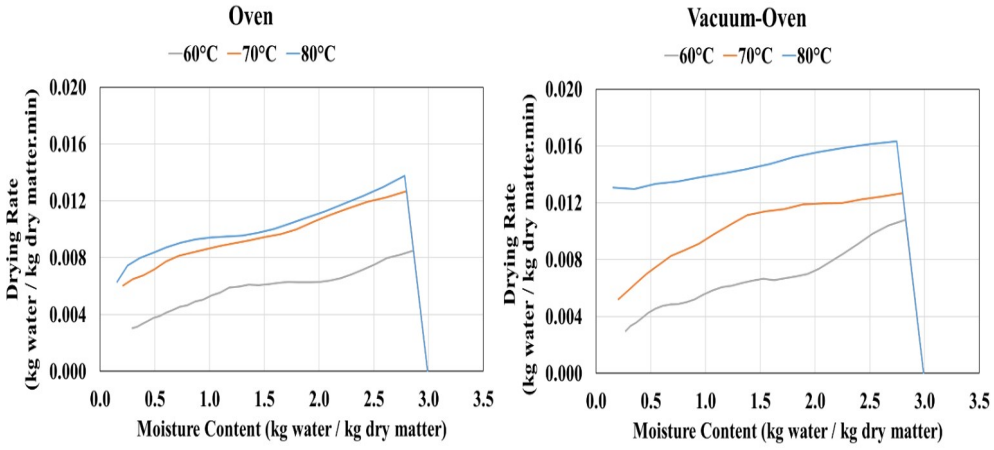

Figure 2: The oven and vacuum oven drying rate curves of golden berries.

3.2. Drying Kinetics: Effective Moisture Diffusivity and Activation Energy Results

For each drying temperature and drying method, D_{eff} values were calculated from the slope of the ln(MR) versus drying time plots, which are presented in Figure 3. The effective moisture diffusivities obtained for each method and for each drying temperature are presented in Figure 4a. As it can be seen from Figure 4a, D_{eff} values calculated for vacuum oven drying are greater than those for oven drying, due to the lower drying times obtained in the presence of vacuum. In oven drying, D_{eff} values were found as 1.95×10^{-10}, 3.37×10^{-10} and 3.80×10^{-10} m^2/s, for drying temperatures of 60, 70, and 80 °C, respectively. On the contrary, in vacuum oven drying, D_{eff} values were found as 2.20×10^{-10}, 3.72×10^{-10} and 5.45×10^{-10} m^2/s, during the experiments performed at 60, 70 and 80 °C, respectively.

Furthermore, in order to calculate the activation energy for the drying processes, D_{eff} values shown in Figure 4a were employed. The plots of $\ln(D_{eff})$ versus 1/T are presented in Figure 4b. From the slopes of the foresaid $\ln(D_{eff})$ versus 1/T plots, the values of E_a were calculated by multiplying the slope with the universal gas constant ($R = 8.314\times10^{-3}$ kJ/mol×K). Accordingly, the activation energies were found as 32.81 and 44.30 kJ/mol, for oven drying and vacuum oven drying, respectively. Since the assistance of vacuum increased the D_{eff} values, the activation energy was also observed to increase during vacuum oven drying.

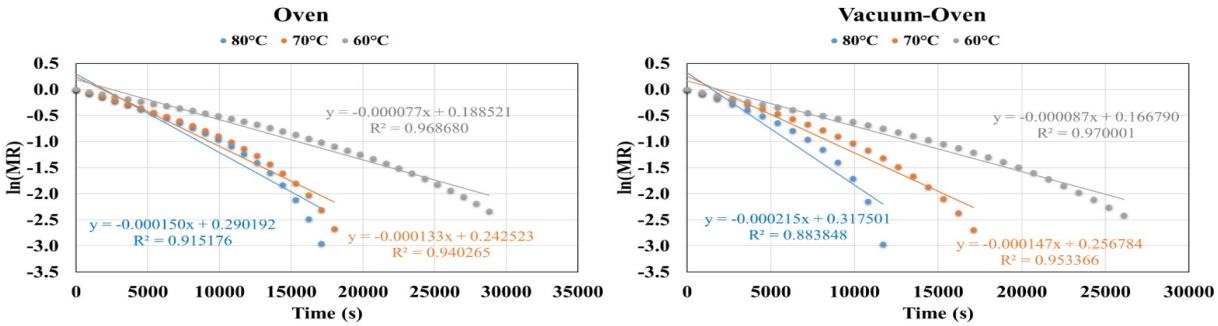

Figure 3: ln(MR) versus drying time plots for oven and vacuum oven drying.

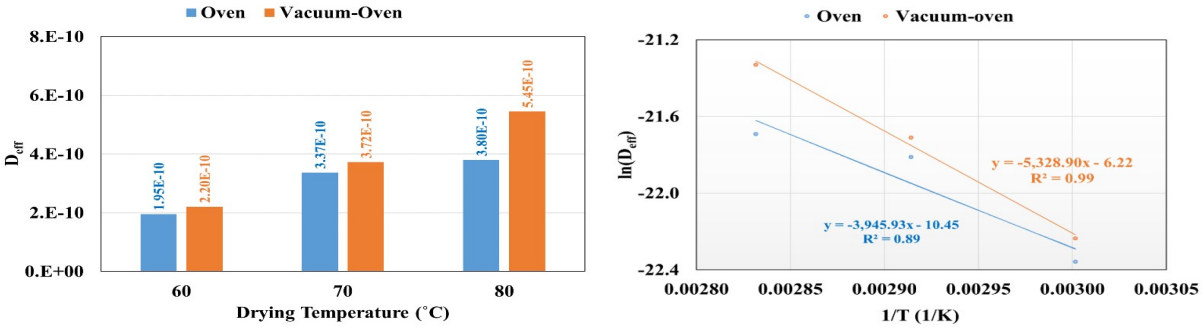

(a) **(b)**

Figure 4: a) D_{eff} values calculated for each drying temperature and drying method. **b)** The plot of $\ln(D_{eff})$ versus 1/T.

3.3. Mathematical Modeling Results

For the mathematical modeling of the drying of golden berries, fourteen mathematical models present in the literature were investigated. Regarding the model parameters and the statistical evaluation results ($R^2 > 0.998$), the models that provided the best fit for oven and vacuum oven drying are presented in Table 2. Among the fourteen mathematical models that were tested five models, namely Aghbashlo et al., Logarithmic, Midilli & Kucuk, Parabolic and Wang & Singh models, gave R^2 values higher than 0.998. For oven drying, the maximum R^2 (between 0.999799 and 0.999957), along with the minimum χ^2 (between 0.000004 and 0.000017) and RMSE (between 0.001879 and 0.003807) values were obtained from the model of Midilli & Kucuk. This model provided the best results for vacuum oven drying as well. Considering Midilli & Kucuk model, for vacuum oven drying of golden berries, R^2 values were between 0.999648 and 0.999998. χ^2 and RMSE values, on the other hand, were less than 0.000001-0.000029 and 0.000378-0.005089, respectively.

Table 2: Drying model constants and statistical parameters (R^2>0.998) for oven drying and vacuum oven drying of golden berries.

		Oven Drying			Vacuum Oven Drying		
Model	**Params**	**60 °C**	**70 °C**	**80 °C**	**60 °C**	**70 °C**	**80 °C**
Aghbashlo et al.	k_1	0.003198	0.003936	0.004039	0.002559	0.004231	0.005051
	k_2	-0.000897	-0.001724	-0.001959	-0.000965	-0.001907	-0.003148
	R^2	0.998865	0.999198	0.998328	0.999698	0.999977	0.998922
	χ^2	0.000088	0.000070	0.000153	0.000024	0.000002	0.000108
	RMSE	0.009057	0.007984	0.011738	0.004718	0.001380	0.009629
Logarithmic	a	1.434928	1.904526	2.205490	1.660257	1.735105	3.734810
	k	0.002295	0.002245	0.001970	0.001669	0.002824	0.001500
	c	-0.444364	-0.905562	-1.211370	-0.659638	-0.722035	-2.734230
	R^2	0.999770	0.999957	0.999908	0.999597	0.999322	0.999997
	χ^2	0.000019	0.000004	0.000009	0.000033	0.000067	<0.000001
	RMSE	0.004081	0.001843	0.002755	0.005446	0.007559	0.000465
Midilli & Kucuk	a	0.997277	0.999061	0.999956	0.990199	0.993081	1.000129
	k	0.003482	0.003167	0.003877	0.001446	0.001754	0.002966
	n	0.962940	1.013221	0.946609	1.099835	1.197080	1.019046
	b	-0.000499	-0.000980	-0.001396	-0.000386	-0.000540	-0.002428
	R^2	0.999799	0.999948	0.999957	0.999648	0.999852	0.999998
	χ^2	0.000017	0.000005	0.000004	0.000029	0.000016	<0.000001
	RMSE	0.003807	0.002036	0.001879	0.005089	0.003535	0.000378
Parabolic	a	0.983405	0.995936	0.991677	0.997178	1.010471	1.000051
	b	-0.003067	-0.004130	-0.004228	-0.002657	-0.004715	-0.005555
	c	0.000002	0.000003	0.000003	0.000002	0.000005	0.000004
	R^2	0.999617	0.999943	0.999856	0.999783	0.999665	0.999996
	χ^2	0.000031	0.000005	0.000014	0.000018	0.000033	<0.000001
	RMSE	0.005259	0.002122	0.003443	0.003999	0.005311	0.000555
Wang & Singh	a	-0.003217	-0.004183	-0.004342	-0.002680	-0.004572	-0.005554
	b	0.000003	0.000004	0.000004	0.000002	0.000004	0.000004
	R^2	0.999135	0.999916	0.999743	0.999769	0.999490	0.999996
	χ^2	0.000067	0.000007	0.000024	0.000018	0.000048	<0.000001
	RMSE	0.007907	0.002591	0.004604	0.004122	0.006557	0.000556

The comparison of the experimental and predicted MR results obtained from the mathematical model of Midilli & Kucuk is presented in Figure 5a for oven drying and in Figure 5b for vacuum oven drying. Regarding the figures, as all of the data lied on the 45° line, it can be concluded that the fitted Midilli & Kucuk model can be excellently used to represent the experimental drying data.

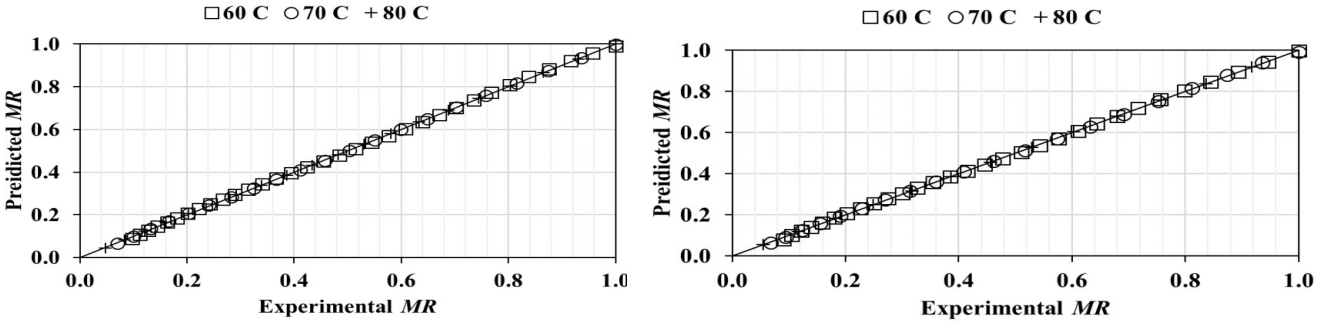

(a) **(b)**

Figure 5: The plot of experimental MR versus predicted MR for Midilli & Kucuk model, in **a)** oven drying and **b)** vacuum oven drying.

4. CONCLUSION

In this study, oven and vacuum oven drying of golden berries were investigated, at drying temperatures of 60, 70, and 80 °C. It was observed that the increase in drying temperature and the assistance of vacuum caused shorter drying times. The duration of drying was between 285-480 minutes for oven drying and between 195-435 minutes for vacuum oven drying, respectively. Taking into account the drying rate curves, for both drying methods, a rapid rising-rate period followed by a falling-rate period was observed. Considering the drying kinetic parameters, the effective moisture diffusivities calculated for oven drying were between 1.95×10^{-10} and 3.80×10^{-10} m^2/s; and for vacuum oven drying were between 2.20×10^{-10} and 5.45×10^{-10} m^2/s. Calculations regarding the activation energy, on the other hand, unveiled 32.81 and 44.30 kJ/mol for oven and vacuum oven drying, respectively. Furthermore, fourteen mathematical models were fitted and tested to represent the drying curve data. Among the tested models Aghbashlo et al., Logarithmic, Parabolic and Wang & Singh models yielded very good fits, having R^2 greater than 0.998. For both oven and vacuum oven drying, Midilli & Kucuk model was found to yield the best fit among the employed models.

4. REFERENCES

Alibas, I. (2014). Microwave, Air and Combined Microwave-Air Drying of Grape Leaves (Vitis vinifera L.) and the Determination of Some Quality Parameters. *International Journal of Food Engineering*, *10*(1), 69–88. https://doi.org/10.1515/ijfe-2012-0037

Amiri Chayjan, R., & Shadidi, B. (2014). Modeling High-Moisture Faba Bean Drying in Fixed and Semi-Fluidized Bed Conditions: MODELING FABA BEAN DRYING IN SEMI-FLUIDIZED BED. *Journal of Food Processing and Preservation*, *38*(1), 200–211. https://doi.org/10.1111/j.1745-4549.2012.00766.x

AOAC International. (1975). *Association of Official Analytical Chemists*. AOAC International.

Başlar, M., Kılıçlı, M., Toker, O. S., Sağdıç, O., & Arici, M. (2014). Ultrasonic vacuum drying technique as a novel process for shortening the drying period for beef and chicken meats. *Innovative Food Science & Emerging Technologies*, *26*, 182–190. https://doi.org/10.1016/j.ifset.2014.06.008

Bravo, K., & Osorio, E. (2016). Characterization of polyphenol oxidase from Cape gooseberry (Physalis peruviana L.) fruit. *Food Chemistry*, *197*, 185–190. https://doi.org/10.1016/j.foodchem.2015.10.126

Calín-Sánchez, Á., Figiel, A., Wojdyło, A., Szarycz, M., & Carbonell-Barrachina, Á. A. (2014). Drying of Garlic Slices Using Convective Pre-drying and Vacuum-Microwave Finishing Drying: Kinetics, Energy Consumption, and Quality Studies. *Food and Bioprocess Technology*, *7*(2), 398–408. https://doi.org/10.1007/s11947-013-1062-3

Crank, J. (1975). *The Mathematics of Diffusion*. Oxford University Press.

Doymaz, I., Kipcak, A. S., & Piskin, S. (2016). Microwave drying of green bean slices: Drying kinetics and physical quality. *Czech Journal of Food Sciences*, *33*(No. 4), 367–376. https://doi.org/10.17221/566/2014-CJFS

Etzbach, L., Meinert, M., Faber, T., Klein, C., Schieber, A., & Weber, F. (2020). Effects of carrier agents on powder properties, stability of carotenoids, and encapsulation efficiency of goldenberry (Physalis peruviana L.) powder produced by co-current spray drying. *Current Research in Food Science*, *3*, 73–81. https://doi.org/10.1016/j.crfs.2020.03.002

Guiné, R. P. F. (2018). The Drying of Foods and Its Effect on the Physical-Chemical, Sensorial and Nutritional Properties. *ETP International*

Journal of Food Engineering, 93–100. https://doi.org/10.18178/ijfe.4.2.93-100

Ismail, O., & Kocabay, O. G. (2018). Evaluation of two fitting methods for thin-layer drying of cape gooseberry fruits. *Turkish Journal of Fisheries and Aquatic Sciences*, *18*(2). https://doi.org/10.4194/1303-2712-v18_2_05

Junqueira, J. R. de J., Corrêa, J. L. G., de Oliveira, H. M., Ivo Soares Avelar, R., & Salles Pio, L. A. (2017). Convective drying of cape gooseberry fruits: Effect of pretreatments on kinetics and quality parameters. *LWT - Food Science and Technology*, *82*, 404–410. https://doi.org/10.1016/j.lwt.2017.04.072

Kaleta, A., & Górnicki, K. (2010). Some remarks on evaluation of drying models of red beet particles. *Energy Conversion and Management*, *51*(12), 2967–2978. https://doi.org/10.1016/j.enconman.2010.06.040

Karacabey, E. (2016). Evaluation of Two Fitting Methods Applied for Thin-Layer Drying of Cape Gooseberry Fruits. *Brazilian Archives of Biology and Technology*, *59*(0). https://doi.org/10.1590/1678-4324-2016160470

Kipcak, A., Derun, E., Tugrul, N., & Doymaz, İ. (2021). Drying characteristics of blue mussels by traditional methods. *Chemical Industry and Chemical Engineering Quarterly*, *27*(3), 279–288. https://doi.org/10.2298/CICEQ200920046K

Lopez, J., Vega-Gálvez, A., Torres, M. J., Lemus-Mondaca, R., Quispe-Fuentes, I., & Di Scala, K. (2013). Effect of dehydration temperature on physico-chemical properties and antioxidant capacity of goldenberry (Physalis peruviana L.). *Chilean Journal of Agricultural Research*, *73*(3), 293–300. https://doi.org/10.4067/S0718-58392013000300013

Nawirska-Olszańska, A., Stępień, B., Biesiada, A., Kolniak-Ostek, J., & Oziembłowski, M. (2017). Rheological, Chemical and Physical Characteristics of Golden Berry (Physalis peruviana L.) after Convective and Microwave Drying. *Foods*, *6*(8), 60. https://doi.org/10.3390/foods6080060

Ozyalcin, Z. O., & Kipcak, A. S. (2020). The Effect of Ultrasonic Pre-Treatment on the Temperature Controlled Infrared Drying of Loligo Vulgaris and Comparison with the Microwave Drying. *Turkish Journal of Fisheries and Aquatic Sciences*, *21*(03), 135–145. https://doi.org/10.4194/1303-2712-v21_3_04

Pan, Z., Khir, R., Godfrey, L. D., Lewis, R., Thompson, J. F., & Salim, A. (2008). Feasibility of simultaneous rough rice drying and disinfestations by infrared radiation heating and rice milling quality. *Journal of Food Engineering*, *84*(3), 469–479. https://doi.org/10.1016/j.jfoodeng.2007.06.005

Puente, L., Vega-Gálvez, A., Fuentes, I., Stucken, K., Rodríguez, A., & Pastén, A. (2021). Effects of drying methods on the characterization of fatty acids, bioactive compounds and antioxidant capacity in a thin layer of physalis (Physalis peruviana L.) pulp. *Journal of Food Science and Technology*, *58*(4), 1470–1479. https://doi.org/10.1007/s13197-020-04659-0

Ramadan, M. F. (2011). Bioactive phytochemicals, nutritional value, and functional properties of cape gooseberry (Physalis peruviana): An overview. *Food Research International*, *44*(7), 1830–1836. https://doi.org/10.1016/j.foodres.2010.12.042

Uribe, E., Gómez-Pérez, L. S., Pasten, A., Pardo, C., Puente, L., & Vega-Galvez, A. (2022). Assessment of refractive window drying of physalis (Physalis peruviana L.) puree at different temperatures: Drying kinetic prediction and retention of bioactive components. *Journal of Food Measurement and Characterization*, *16*(4), 2605–2615. https://doi.org/10.1007/s11694-022-01373-7

Vega-Gálvez, A., Puente-Díaz, L., Lemus-Mondaca, R., Miranda, M., & Torres, M. J. (2014). Mathematical Modeling of Thin-Layer Drying Kinetics of Cape Gooseberry (*Physalis peruviana* L.): Drying of Cape Gooseberry (*Physalis peruviana* L.). *Journal of Food Processing and Preservation*, *38*(2), 728–736. https://doi.org/10.1111/jfpp.12024

Zhu, A. (2018). The convective hot air drying of *Lactuca sativa* slices. *International Journal of Green Energy*, *15*(3), 201–207. https://doi.org/10.1080/15435075.2018.1434523

JOTCS B
Journal of the Turkish Chemical Society
Section: B
Chemical Engineering
TURKISH CHEMICAL SOCIETY

Obtaining Diatomite Reinforced Epoxy Composite and Determination of Its Thermophysical Properties

Mustafa DAĞ

[1]Chemical Engineering, Engineering Faculty, Çankırı Karatekin University, Çankırı, Türkiye,

Abstract: In this research, a composite material was produced by adding diatomite soil to epoxy resin. The particle size of the diatomite used is in the range of 297 to 149 microns. It was dried at 378 K before being used as a filling material. By adding 0 kg, 0.001 kg, 0.002 kg, 0.004 kg, and 0.006 kg of diatomite to the epoxy matrix, the composite was produced under atmospheric conditions. To obtain a homogeneous structure, certain amounts of Epoxy A component and diatomite were mixed first. A selected amount of epoxy component B was then added to the mixture. After one day of curing in the laboratory, necessary tests and analyses were carried out. The surface morphology of the produced composite was examined by scanning electron microscopy (SEM). As a result of the analyses and tests, it was seen that the increase in the amount of diatomite increased the porosity in the composite. In addition, it was observed that the density decreased, and the thermal conductivity coefficient varied between 0.110 W /m.K and 0.095 W /m.K It was observed that the hardness was linearly in the range of 77-80 shore D. It has been determined that the addition of diatomite tends to increase the activation energy by modeling the thermal degradation experiments performed in the PID controlled system in nitrogen environment between 300 K and 900 K. Activation energy values are calculated according to the one-dimensional diffusion function with the highest correlation coefficient (R^2) according to Coats-Redfern method when the temperature rise is 10 K/min, and the conversion rate (α) is between 0.15 and 0.85.

Keywords: Diatomite, Epoxy Composite, Density, Hardness, Thermal Conductivity.

Submitted: September 13, 2022. **Accepted:** December 27, 2022.

Cite this: Dağ, M. (2023). Obtaining Diatomite Reinforced Epoxy Composite and Determination of Its Thermophysical Properties. Journal of the Turkish Chemical Society, Section B: Chemical Engineering, 6(1), 9–16.

***Corresponding author. E-mail:** mudag@karatekin.edu.tr.

1. INTRODUCTION

Due to the increase in the need for raw materials in proportion to today's technology, which is defined as the age of science, industry has led to the fact that it continues to search for resources at an increasing rate. The limited resources in the world and the lack of sustainable features of existing resources force researchers to develop renewable resources. In this context, the use of natural minerals and ores in nature as well as bio-resources is one of the driving forces of the solutions found for this resource generation. As another type of solution, it can also be said that the development of materials with different properties and the number of properties can be increased. It can be said that the development and production of composite materials with multiple properties is of vital importance to keep up with the speed of technology developing with innovation and to take maximum advantage of limited resources. Although the origin of composites dates back thousands of years and the first composites consisted of mud bricks mixed with straw, their importance has become more understandable in recent years. In addition, it is known from the literature that developed countries have devoted significant resources to the development and production of sustainable and renewable composites in recent years. The properties of composites are generally; low density, wear resistance, favorable fatigue and toughness properties, energy saving, low cost, resistance to oxidation, etc. can be mentioned. Its usage areas can be counted as military technologies, automotive industry, aviation, space technologies, clothing, packaging, medicine, and cleaning products. Such as the superior properties of composites, the cost of raw materials, the precision of production methods, and forming problems also have weak properties. In the production of composites, there are three basic

parts, namely matrix, filler, and additive materials. The use of these parts with appropriate materials ensures the production of a composite with the desired properties. Especially at the production stage, a good selection of the matrix element helps to produce a quality composite. Different matrix materials can be used according to different industries (epoxy, polyurethane, polyester, etc.). The matrix element in question in this study is epoxy resin. The superior properties of epoxy resin can be said as the reasons for using it. The density of the epoxy resin is 1140 kg/m^3 at 298 K. The hardness of the epoxy resin takes a value between 70-90 in terms of shore D, depending on the condition of the material. In addition, the thermal conductivity of the epoxy resin can be between 0.15-0.2 W/m.K. These features can be said as excellent adhesiveness, chemical and thermal resistance, electrical insulation, thermoset resin property, chemical stability, low cost, curing shrinkage, and good mechanical properties. Due to these characteristics, it has a wide range of uses from aviation to the energy industry, from the construction sector to adhesives, and from marine vehicles to installation materials (Arat et al., 2022; Aydoğmuş, 2022; Aydoğmuş et al., 2022a, 2022b; Dağ et al., 2022; George & Bhattacharyya, 2021; İNal & Ataş, 2018, 2018; Kaya, 2016; Özdemir, 2019; Şahal & Aydoğmuş, 2021; Yalçın, 2010; Yanen et al., 2022). In the literature, it has been seen that inorganic or organic filling materials such as graphene, nano silica, nanoclay, polyimide, cellulose nanofiber, etc. are added to epoxy matrices to impart various properties. Apart from the outstanding properties of epoxy resins, there are also various weaknesses. Due to the three-dimensional network structure, high internal stress, high brittleness, poor fatigue resistance, microcrack formation, strength reduction during the high-temperature curing process, etc. can be counted. In this context, the study of eliminating weak properties by adding some additives and fillers continues to research. Epoxy resins are produced by the reaction of crosslinking monomers with curing agents during production. The epoxies used in the market are bisphenol A (BPA) based industrially produced petroleum-based resins. The use of petroleum-based ones in European and American continental countries is increasingly hindered since they cause health problems. Studies are continuing the elimination of harmful properties in composite production (Chen et al., 2019; Dahmen et al., 2020; Guo et al., 2021; Huang et al., 2012; Koo et al., 2016; Li et al., 2018; Ma et al., 2019; Mantecón et al., 1987; Pathak et al., 2016; Rad et al., 2019; Seachrist et al., 2016; Serra et al., 1986; Sogancioglu et al., 2017; Sun et al., 2014, 2015, 2020; Wongjaiyen et al., 2018; Xu et al., 2018; Yang et al., 2020). In recent years, research has been conducted on the use of diatomite in composite production. The most striking physical property of diatomite is its high porosity and low specific gravity. The thermal conductivity of diatomite is approximately 0.09 W/m^2 at low temperatures. This low thermal conductivity is explained by the porous structure and low density of diatomite. The specific gravity of the dry diatomite has a value between 150 and 400 kg/m^3. Diatomite also has properties such as being in the form of $SiO_2.nH_2O$, being abundant, has a high-water holding capacity, having a hardness of 1.5-6 Mohs, and is abrasive. It also suggests that due to its high chemical resistance, it will help to give the desired properties to composite material (Davis et al., 2016; Karaman et al., 2011; Qi et al., 2007; Qin et al., 2015; Taş & Çetin, 2012; Wang et al., 2015; Zhang et al., 2017) (33-39). In this study, it was aimed to produce diatomite added composite, which is a material of organic origin, by adding diatomite to epoxy resin. In addition, it is aimed to produce more effective composites by utilizing the superior properties of diatomite such as high porosity and low specific gravity.

2. MATERIAL AND METHOD

Epoxy A and Epoxy B components used in experimental studies were supplied by Turkuaz Polyester company. In addition, diatomite used as a filler was purchased from the Turkish diatom company. Diatomite is added to the epoxy resin A at different rates (0 wt.%, 1 wt.%, 2 wt.%, 4 wt.%, and 6 wt.%) and mixed at 1000 rpm for 5 min.

After adding epoxy resin B, respectively, at room temperature at a mixing speed of 1200 rpm for 90 seconds, they are poured into standard molds. After waiting 24 hours for the curing of the obtained samples, necessary tests and analyses have been carried out. In addition, mold release agents are applied to standard steel cylindrical molds, allowing the samples to come out easily. In Figure 1, the epoxy composite production scheme in experimental studies is expressed. Here, both the quantities of the ingredients and the order of use are very important. Also, the fillers should provide a homogeneous distribution to the synthesized composite.

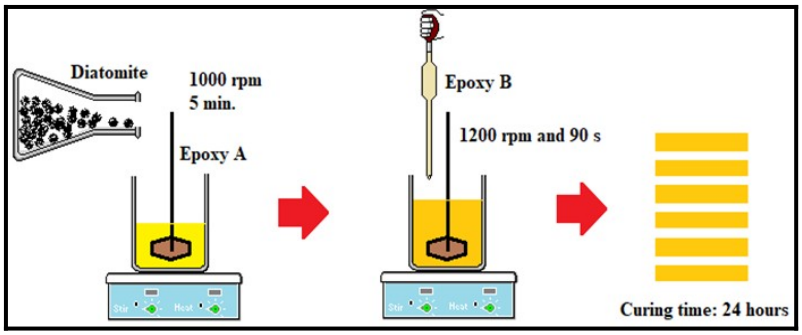

Figure 1: Production scheme of diatomite reinforced epoxy composite.

The amounts of each ingredient used are expressed in Table 1. The amounts of other components are kept constant, except for the filler (diatomite) used here.

Table 1: Production plan of diatomite-reinforced epoxy composite.

Epoxy A (kg)	Epoxy B (kg)	Diatomite (kg)
0.067	0.033	0
0.067	0.033	0.001
0.067	0.033	0.002
0.067	0.033	0.004
0.067	0.033	0.006

The devices and standards used for analyses in experimental studies are as follows: Shore D hardness tests have been carried out by the ISO 868 (ASTM D 2240) standard, and dielectric properties have been measured with the Novacontrol Alpha-A impedance analyzer at a temperature of 300 K in the frequency range of 10 Hz and 10 MHz.

3. RESULTS AND DISCUSSIONS

The variation of the density of the obtained epoxy composites is shown in Figure 2 depending on the diatomite ratio by mass. It is understood from the graph that diatomite reduces the density of the epoxy composite linearly. Obtaining a linear graphic can be interpreted as an indication that the mixture is homogeneous and well dispersed. When the distribution is not good, graphs with parabolic or different features are obtained in positive or negative directions. Based on the literature, it can be said that the addition of diatomite, which has a lower density than the epoxy resin, to the epoxy caused a tendency to decrease the density of the epoxy. For this reason, increasing the diatomite ratio played an active role in reducing the density of other samples.

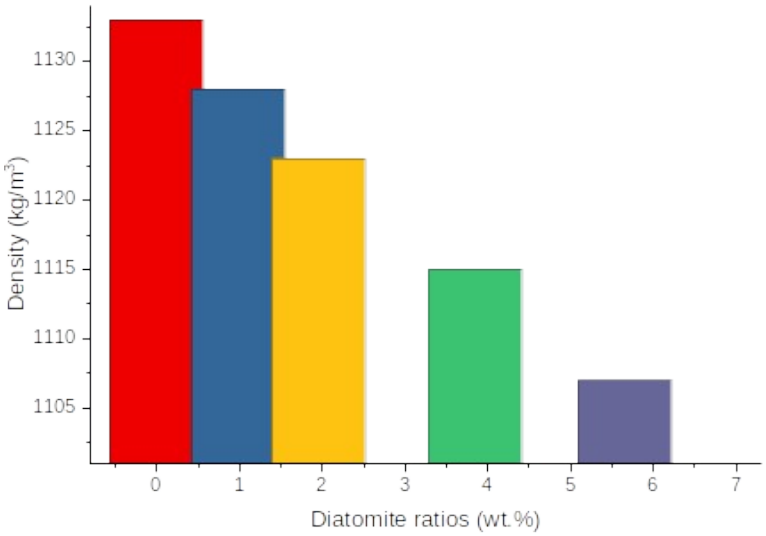

Figure 2: The effect of diatomite reinforcement on the density of epoxy composite.

In the graphs shown in Figure 3, it is seen that the hardness of the synthesized epoxy composites increased with diatomite reinforcement. Shore hardness unit is used to determine the hardness value of polymer or flexible materials, while Mohs hardness unit is used for the hardness value of ores or minerals. It is known in the literature that epoxy resins have a hardness between 70-90 as shore D. The hardness of diatomite is between 1.5 and 6 in Mohs. As can be seen in Figure 3, while pure epoxy Shore D is at the value of 77, it is seen that this value increases as the proportion of diatomite added to it raises. this suggests that this is since diatomite provides good physical adhesion during uniform dispersion in epoxy resin. Because Mohs hardness is based on the principle of measuring the hardness by drawing the sample. the deeper a sample is drawn, the less its hardness. The deep lines of the diatomite, which has a Mohs hardness of 1.5-6, formed good physical bonds with the epoxy and this can be interpreted as an increase in the hardness of the composite. As it is known, the more roughness there is in a material, the more adhesion and adhesion occur. Considering the adhesive properties of epoxy resins, this result has contributed to the accuracy of the interpretation.

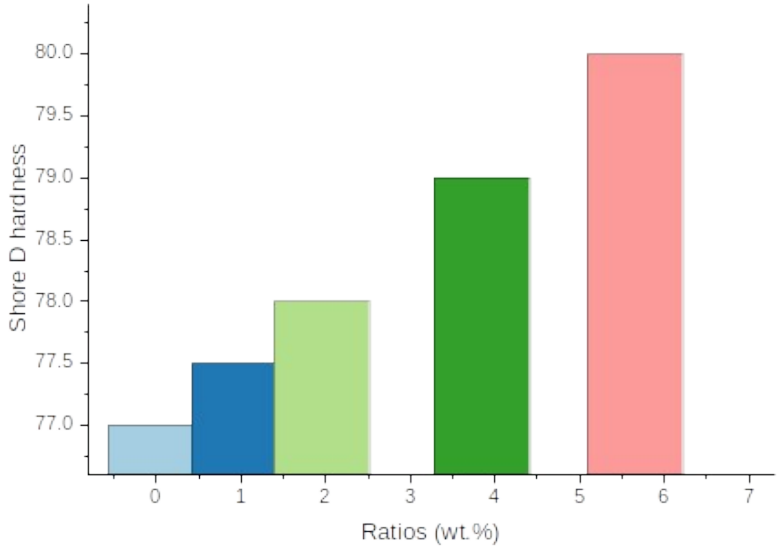

Figure 3: The effect of diatomite reinforcement on the hardness of the epoxy composite.

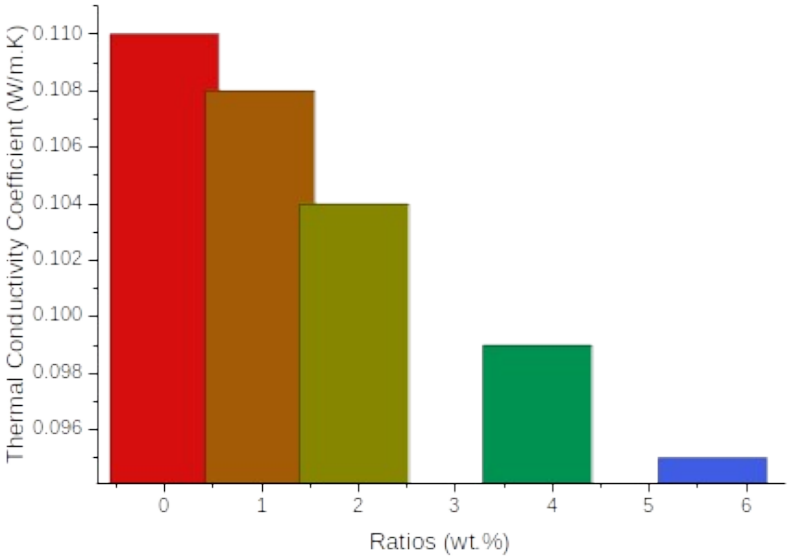

Figure 4: The effect of diatomite reinforcement on the thermal conductivity of the epoxy composite.

It is seen from the literature that the thermal conductivity of epoxy resin is between 0.15-0.2 W/m.K. The thermal conductivity of the diatomite added as an additive is approximately 0.09 W/m.K. When Graph 4 is examined, it is seen that while the thermal conductivity value of pure epoxy is 0.11 W/m.K, as the diatomite added to the composite increases, the thermal value gradually decreases, very close to the linear characteristic. The fact that the graph is close to linearity can be interpreted as

a good mix and distribution, but not fully linear due to the effect of different reasons. As other reasons, it is thought that air gaps remain in the parts of the diatomite which have a porous structure in the inner regions during mixing and the thermal conductivity in the mortar affects the total thermal conductivity value. In addition, although the curing time is expected to be 24 hours, it is thought that there is no escape of air from the diatomites in the inner regions. It is also possible for the epoxy matrix to absorb air during mixing at 1000-1200 rpm.

Activation energy (*Ea*) values are calculated according to Coats-Redfern (Table 2). Activation energy (*Ea*), Arrhenius constant (*A*), and temperature rise rate (β) values were expressed. Coats-Redfern (Eq. 9) model are shown in the below equations.

$$\ln\left(\frac{g(\alpha)}{T^2}\right)=\ln\frac{AR}{Ea\beta}-\frac{Ea}{RT} \quad \text{(Eq. 1)}$$

Plotting *1/T* versus ln($g(\alpha)/T^2$) according to Coats-Redfern method, the slope will give the value *-Ea/R*. Since the value of R = 8.314 J/mol·K here, the slope can be easily calculated. Coats-Redfern method has been preferred because it found the most compatible results with the n-order function. In this method, the highest correlation coefficient was obtained with three-dimensional diffusion equation. Activation energies of the pure epoxy and epoxy composites reinforced with fillers are calculated in thermal decomposition experiments carried out at a heating rate of about 10 K/min at 878 K.

Table 2: Activation energies of pure and diatomite reinforced epoxy composites.

Ratio (wt.%)	Activation Energy (kJ/mol)
0	185.26
0.99	189.65
1.96	194.70
3.85	199.86
5.66	207.43

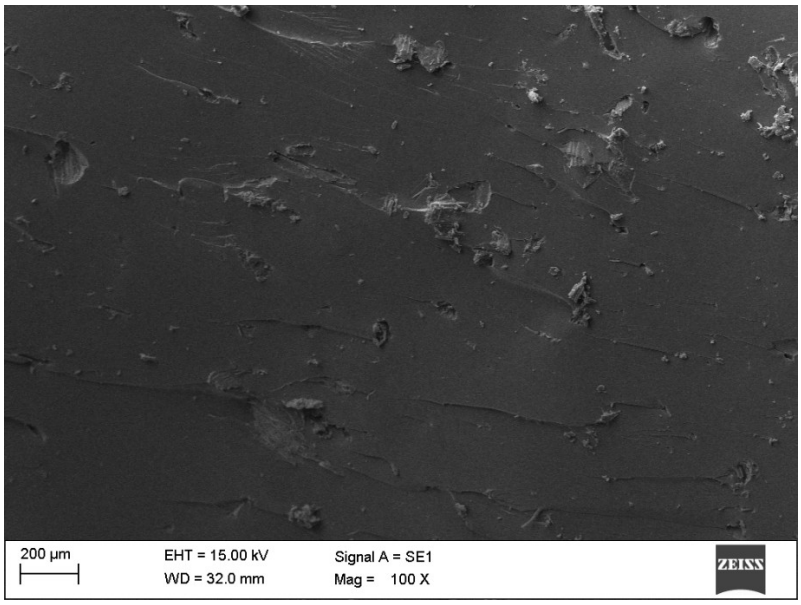

Figure 5: SEM image of diatomite (5.66 wt.%) reinforced epoxy composite.

In the SEM image, it was observed that the addition of diatomite increased the number of pores in the epoxy resin. Here, the addition of 5 percent diatomite led to the appearance of prominent pores. It is known from the literature that the SEM images of pure epoxy resin are in the form of a non-porous and flat surface. Here, it was observed that the pores started to appear in the diatomite additive at a low percentage. It is of no doubt that denser pores will be seen with the increase in the diatomite percentage. It has been observed in some experiments that the diatomite layer above a certain ratio causes irreversible breaks and cracks on the epoxy resin. The porosity of the matrix can provide significant advantages compared to the areas to be used (Conradi et al., 2020).

4 .CONCLUSIONS

In this study, a composite material was produced by adding diatomite to epoxy resin. Various tests were carried out on composite materials prepared by adding different amounts of diatomite. As a result of these tests, with the addition of diatomite, results were obtained in the form of a decrease in the density of the epoxy matrix, an increase in its thermal conductivity, and a low-slope linear increase in its hardness. When the SEM image is examined, it can be considered that the increase in porosity is the reason for the decrease in density. The increase in porosity also indirectly affected the thermal conductivity. It has been observed that it reduces the thermal conductivity by 13 percent. The increase in the activation energy can be interpreted as the addition of diatomite increases the thermal stability on the epoxy resin. As suggestions for future studies, the following points can be drawn: Lower diatomite sizes can be used in the matrix to reduce porosity, the effect of temperature can be examined by producing in different temperature environments, trials can be carried out with a second or third matrix partnership with epoxy resin.

5. ACKNOWLEDGMENT

The author thanks Çankırı Karatekin University Chemical Engineering Department and Scientific Research Projects Coordinatorship (BAP) for their support in laboratory studies.

6. REFERENCES

Arat, A. Y., Kaya, H., & Baş Çep, E. (2022). Grafenli ve geri dönüştürülmüş karbon fiberli polimer kompozit malzemenin üretilerek mekanik deney çubuklarının üretimi ve incelenmesi. *ImasCongress*, 323–329.

Aydoğmuş, E. (2022). Biohybrid nanocomposite production and characterization by RSM investigation of thermal decomposition kinetics with ANN. *Biomass Conversion and Biorefinery*, *12*(10), 4799–4816. https://doi.org/10.1007/s13399-022-02403-6

Aydoğmuş, E., Dağ, M., Yalçın, Z. G., & Arslanoğlu, H. (2022a). Synthesis and characterization of EPS reinforced modified castor oil-based epoxy biocomposite. *Journal of Building Engineering*, *47*, 103897. https://doi.org/10.1016/j.jobe.2021.103897

Aydoğmuş, E., Dağ, M., Yalçın, Z. G., & Arslanoğlu, H. (2022b). Synthesis and characterization of waste polyethylene reinforced modified castor oil-based polyester biocomposite. *Journal of Applied Polymer Science*, *139*(27). https://doi.org/10.1002/app.52526

Chen, Y., Sui, L., Fang, H., Ding, C., Li, Z., Jiang, S., & Hou, H. (2019). Superior mechanical enhancement of epoxy composites reinforced by polyimide nanofibers via a vacuum-assisted hot-pressing. *Composites Science and Technology*, *174*, 20–26. https://doi.org/10.1016/j.compscitech.2019.02.012

Conradi, M., Kocijan, A., Kosec, T., & Podgornik, B. (2020). Manipulation of TiO2 Nanoparticle/Polymer Coatings Wettability and Friction in Different Environments. *Materials*, *13*(7), 1702. https://doi.org/10.3390/ma13071702

Dağ, M., Yanen, C., & Aydoğmuş, E. (2022). Bor Fabrikası Bileşenlerinin Epoksi Kompozitin Termofiziksel Özelliklerine Etkisi. *European Journal of Science and Technology*. https://doi.org/10.31590/ejosat.1108402

Dahmen, V., Redmann, A. J., Austermann, J., Quintanilla, A. L., Mecham, S. J., & Osswald, T. A. (2020). Fabrication of hybrid composite T-joints by co-curing with 3D printed dual cure epoxy. *Composites Part B: Engineering*, *183*, 107728. https://doi.org/10.1016/j.compositesb.2019.107728

Davis, S., Mohandas, S., Nzoumba, G., & Yancey, T. (2016). Diatomite in Upper Eocene Jackson Group, Fayette County, Texas. *Gulf Coast Association of Geological Societies Transactions*, *66*, 739–746.

George, J., & Bhattacharyya, D. (2021). Biocarbon reinforced polypropylene composite: An investigation of mechanical and filler behavior through advanced dynamic atomic force microscopy and X-ray micro CT. *Express Polymer Letters*, *15*(3), 224–235. https://doi.org/10.3144/expresspolymlett.2021.20

Guo, L., Huang, J., Zhang, L., & Sun, X. (2021). Damage evolution of 3D woven carbon/epoxy composites under tension-tension fatigue loading based on synchrotron radiation computed tomography (SRCT). *International Journal of Fatigue*, *142*, 105913. https://doi.org/10.1016/j.ijfatigue.2020.105913

Huang, Y. Q., Wong, C. K. C., Zheng, J. S., Bouwman, H., Barra, R., Wahlström, B., Neretin, L., & Wong, M. H. (2012). Bisphenol A (BPA) in China: A review of sources, environmental levels, and potential human health impacts. *Environment International*, *42*, 91–99. https://doi.org/10.1016/j.envint.2011.04.010

İnal, O., & Ataş, A. (2018). Kıvrımsız Cam Elyaf Takviyeli Kompozit Plakalarda Pim Bağlantılarının Deneysel Olarak İncelenmesi. *Gazi Üniversitesi Mühendislik-Mimarlık Fakültesi Dergisi*, *2018*(2018). https://doi.org/10.17341/gazimmfd.416441

Karaman, S., Karaipekli, A., Sarı, A., & Biçer, A. (2011). Polyethylene glycol (PEG)/diatomite composite as a novel form-stable phase change material for thermal energy storage. *Solar Energy Materials and Solar Cells*, *95*(7), 1647–1653. https://doi.org/10.1016/j.solmat.2011.01.022

Kaya, A. İ. (2016). Kompozit malzemeler ve özellikleri. *Putech & Composite Poliüretan ve Kompozit Sanayi Dergisi*, *29*, 38–45.

Koo, B., Subramanian, N., & Chattopadhyay, A. (2016). Molecular dynamics study of brittle fracture in epoxy-based thermoset polymer. *Composites Part B: Engineering*, *95*, 433–439. https://doi.org/10.1016/j.compositesb.2016.04.012

Li, Z., Guo, L., Zhang, L., & Wang, Q. (2018). In situ experimental investigation on the out-plane damage evolution of 3D woven carbon-fiber reinforced composites. *Composites Science and Technology*, *162*, 101–109. https://doi.org/10.1016/j.compscitech.2018.04.024

Ma, Y., Liu, H., Wu, J., Yuan, L., Wang, Y., Du, X., Wang, R., Marwa, P. W., Petlulu, P., Chen, X., & Zhang, H. (2019). The adverse health effects of bisphenol A and related toxicity mechanisms. *Environmental Research*, *176*, 108575. https://doi.org/10.1016/j.envres.2019.108575

Mantecón, A., Cádiz, V., Serra, A., & Martínez, P. A. (1987). Curing of N,N′-diglycidylimides with polyfunctional compounds. *European Polymer Journal*, *23*(6), 481–488. https://doi.org/10.1016/0014-3057(87)90140-6

Özdemir, Y. (2019). *Biyo-kompozit Malzemelerin Mekanik Özelliklerinin Geliştirilmesi* [PhD Thesis, Marmara University]. https://avesis.marmara.edu.tr/yonetilen-tez/5f439633-83bf-4095-9a6d-eb0773798297/biyo-kompozit-malzemelerin-mekanik-ozelliklerinin-gelistirilmesi

Pathak, A. K., Borah, M., Gupta, A., Yokozeki, T., & Dhakate, S. R. (2016). Improved mechanical properties of carbon fiber/graphene oxide-epoxy hybrid composites. *Composites Science and Technology*, *135*, 28–38. https://doi.org/10.1016/j.compscitech.2016.09.007

Qi, X., Liu, M., Chen, Z., & Liang, R. (2007). Preparation and properties of diatomite composite superabsorbent. *Polymers for Advanced Technologies*, *18*(3), 184–193. https://doi.org/10.1002/pat.847

Qin, Y., Leng, G., Yu, X., Cao, H., Qiao, G., Dai, Y., Zhang, Y., & Ding, Y. (2015). Sodium sulfate–diatomite composite materials for high temperature thermal energy storage. *Powder Technology*, *282*, 37–42. https://doi.org/10.1016/j.powtec.2014.08.075

Rad, E. R., Vahabi, H., de Anda, A. R., Saeb, M. R., & Thomas, S. (2019). Bio-epoxy resins with inherent flame retardancy. *Progress in Organic Coatings*, *135*, 608–612. https://doi.org/10.1016/j.porgcoat.2019.05.046

Şahal, H., & Aydoğmuş, E. (2021). PRODUCTION AND CHARACTERIZATION OF PALM OIL BASED EPOXY BIOCOMPOSITE BY RSM DESIGN. *Hittite Journal of Science and Engineering*. https://doi.org/10.17350/HJSE19030000241

Seachrist, D. D., Bonk, K. W., Ho, S.-M., Prins, G. S., Soto, A. M., & Keri, R. A. (2016). A review of the carcinogenic potential of bisphenol A. *Reproductive Toxicology*, *59*, 167–182. https://doi.org/10.1016/j.reprotox.2015.09.006

Serra, A., Cádiz, V., Martínez, P.-A., & Mantecón, A. (1986). Preparation and reactivity of new 3,3′,4,4′-tetracarboxybenzophenone dianhydride glycidyl ester derivatives. *Angewandte Makromolekulare Chemie*, *140*(1), 113–125. https://doi.org/10.1002/apmc.1986.051400109

Soganciogl u, M., Yucel, A., Yel, E., & Ahmetli, G. (2017). Production of Epoxy Composite from the Pyrolysis Char of Washed PET Wastes. *Energy Procedia*, *118*, 216–220. https://doi.org/10.1016/j.egypro.2017.07.022

Sun, T., Fan, H., Wang, Z., Liu, X., & Wu, Z. (2015). Modified nano Fe2O3-epoxy composite with enhanced mechanical properties. *Materials & Design*, *87*, 10–16. https://doi.org/10.1016/j.matdes.2015.07.177

Sun, T., Wang, Y., Yang, Y., Fan, H., Liu, M., & Wu, Z. (2020). A novel Fe2O3@APFS/epoxy composite with enhanced mechanical and thermal properties. *Composites Science and Technology*, *193*, 108146. https://doi.org/10.1016/j.compscitech.2020.108146

Sun, T., Wu, Z., Zhuo, Q., Liu, X., Wang, Z., & Fan, H. (2014). Microstructure and mechanical properties of aminated polystyrene spheres/epoxy polymer blends. *Composites Part A: Applied Science and Manufacturing*, *66*, 58–64. https://doi.org/10.1016/j.compositesa.2014.06.015

Taş, B., & Çetin, M. (2012). BİYOLOJİK ORİJİNLİ TEK DOĞAL MİNERAL: DİYATOMİT. *TÜBAV Journal of Science*, *5*(2), 28–46.

Wang, B., de Godoi, F. C., Sun, Z., Zeng, Q., Zheng, S., & Frost, R. L. (2015). Synthesis, characterization and activity of an immobilized photocatalyst: Natural porous diatomite supported titania nanoparticles. *Journal of Colloid and Interface Science*, *438*, 204–211. https://doi.org/10.1016/j.jcis.2014.09.064

Wongjaiyen, T., Brostow, W., & Chonkaew, W. (2018). Tensile properties and wear resistance of epoxy nanocomposites reinforced with cellulose nanofibers. *Polymer Bulletin*, *75*(5), 2039–2051. https://doi.org/10.1007/s00289-017-2142-8

Xu, G., Wang, Z., Zeng, T., Cheng, S., & Fang, D. (2018). Mechanical response of carbon/epoxy composite sandwich structures with three-dimensional corrugated cores. *Composites Science and Technology*, *156*, 296–304. https://doi.org/10.1016/j.compscitech.2018.01.015

Yalçın, K. A. (2010). *Nanoteknoloji ve gıda sanayiinde uygulama alanları* [Master's Thesis, Namık Kemal University]. http://acikerisim.nku.edu.tr:8080/xmlui/bitstream/handle/20.500.11776/657/0031677.pdf?sequence=1

Yanen, C., Dağ, M., & Aydoğmuş, E. (2022). Investigation of Thermophysical Properties of Colemanite, Ulexite, and Tincal Reinforced Polyester Composites. *European Journal of Science and Technology*. https://doi.org/10.31590/ejosat.1108386

Yang, X., Zhu, J., Yang, D., Zhang, J., Guo, Y., Zhong, X., Kong, J., & Gu, J. (2020). High-efficiency improvement of thermal conductivities for epoxy composites from synthesized liquid crystal epoxy followed by doping BN fillers. *Composites Part B: Engineering*, *185*, 107784. https://doi.org/10.1016/j.compositesb.2020.107784

Zhang, G., Sun, Z., Duan, Y., Ma, R., & Zheng, S. (2017). Synthesis of nano-TiO 2 /diatomite composite and its photocatalytic degradation of gaseous formaldehyde. *Applied Surface Science*, *412*, 105–112. https://doi.org/10.1016/j.apsusc.2017.03.198

JOTCS B
Journal of the Turkish Chemical Society Section: B Chemical Engineering
TURKISH CHEMICAL SOCIETY

Composite Cryogels for Drug Delivery Applications: A Preliminary Study with Dye as a Model Drug

Didem Demir[1], Seda Ceylan[2], Nimet Bölgen[3]*

[1]Chemistry and Chemical Process Technologies Department, Mersin Tarsus Organized Industrial Zone Technical Sciences Vocational School, Tarsus University, Mersin, 33100, Türkiye

[2]Bioengineering Department, Faculty of Engineering, Adana Alpaslan Türkeş Science and Technology University, Adana, 01250, Türkiye

[3]Chemical Engineering Department, Faculty of Engineering, Mersin University, Mersin, 33110, Türkiye

Abstract: Cryogels are suitable candidates to be used as drug release systems due to their interconnected pore structures, high surface areas, high liquid absorption capacities, and elasticity. With this purpose, we aimed to produce a cryogel structure to be used in drug release applications with the approach of tissue engineering. As biodegradable and biocompatible polymers chitosan and gelation were selected. The cryogels were fabricated using the combination of these polymers in the presence of glutaraldehyde under cryogenic conditions. The produced optimum gel scaffold was first characterized using FTIR, SEM, porosity, swelling ability, and degradation analyses. Successfully crosslinked gels exhibited an interconnected pore structure with an average pore diameter of 52.95 µm. As a result of the examination of the time-dependent weight change, it was also revealed that the cryogels have a liquid absorption capacity of about 500 times their dry weight and are biodegradable. The mainly characterized cryogel sample was evaluated for potential drug loading and release applications using methyl orange (MO) as a model drug. Gels, which swell in a short time, absorb the dye quickly and the cumulative release of the dye indicates that the gels are suitable for extended-release systems.

Keywords: Chitosan, gelatin, cryogel, drug delivery.

Submitted: November 04, 2022. **Accepted:** February 05, 2023.

Cite this: Demir, D., Ceylan, S., & Bölgen, N. (2023). Composite Cryogels for Drug Delivery Applications: A Preliminary Study with Dye as a Model Drug. Journal of the Turkish Chemical Society, Section B: Chemical Engineering, 6(1), 17–26.

DOI: https://doi.org/10.58692/jotcsb.1199436.

***Corresponding author. E-mail:** nimetbolgen@yahoo.com.

1. INTRODUCTION

The main goal of tissue engineering is restoring, repairing, and maintaining damaged tissue functions with cells, scaffolds, and growth factors (Biondi et al., 2008). Recently, incorporating different drugs (drug active ingredients, small molecule chemicals, proteins, growth factors, cytokines, and other bioactive molecules) into tissue engineering scaffolds has gained a lot of attention, and has great potential in biomedical applications (Mondal et al., 2016). Drug delivery or device system provides optimum dose control on the specific targeted tissues and also decreases the side effects of drugs on the non-targeted tissues as compared to the traditional drug delivery treatments (Yusop et al., 2018). In other words, the selectivity ability of drugs in treating targeted cells for disease treatment is important to protect healthy parts of the body (Surya et al., 2020). In light of this knowledge, the porous structure of the scaffolds has been loaded with various drug types such as painkillers, anti-inflammatory, antimigraine and anti-cancer agents and hormones (Piazzini et al., 2019). Hydrophobic and hydrophilic model drugs (PKH26 or PKH67, methyl orange, methylene blue, etc.) have also been loaded into scaffolds (Kim et al., 2005). In

recent years, using natural or synthetic polymers has attracted wide attention in producing different types of scaffolds and combining them with drugs. Various scaffold production techniques, such as gas foaming, electrospinning, thermal phase separation, emulsification, solvent casting, freeze drying, cryogelation, etc., are used to produce scaffolds. Natural (silk, chitosan, gelatin, starch, pectin, cellulose, etc.) and synthetic polymers (poly (vinyl alcohol) (PVA), poly (lactic-co-glycolic acid) (PLGA), poly-L-lactide (PLA), etc.) based scaffolds obtained by using different techniques have been reported for controlled drug delivery applications in various studies (Shera et al., 2018; Wang et al., 2019). Curcumin-loaded PLGA particles (Yusop et al., 2018), vitamin B12-loaded alginate scaffolds (Bhasarkar & Bal, 2019), recombinant human bone morphogenetic protein 2 and dexamethasone-loaded silk fibroin/PLGA scaffolds (Yao et al., 2019), 5-fluorouracil-loaded nanocellulose/gelatin cryogels (Li et al., 2019) and doxorubicin containing chitosan hydrogel (Han et al., 2008) are impressive examples produced in different researches with updated strategies to design biomimetic scaffolds.

In this study, chitosan and gelatin natural polymers and cryogelation technique were used to produce porous cryogel scaffolds for potential drug loading and release experiments. Chitosan and gelatin are widely used natural polymers due to their favorable properties such as biological compatibility, biodegradability, non-toxicity, and high water absorption capacity (Ayaz et al., 2021). On the other hand, cryogelation is a favorable method to produce three-dimensional structures with highly interconnected porosity (Rogers & Bencherif, 2019). The excellent features of chitosan and gelatin and the use of cryogelation technique are notable for accepting the fabricated scaffolds as excellent candidates for biomedical applications. Up to now, in different research studies, chitosan and gelatin have been incorporated as implantable scaffolds such as wound dressing, bone tissue engineering, neural regeneration, and vehicles for controlled delivery of therapeutic molecules (drug, protein, gene, etc.) (Bhat et al., 2011; Kemençe & Bölgen, 2017, 2017; Lu et al., 2004; Nagahama et al., 2009). Our study aims to reveal the drug loading and release potential of scaffolds prepared in a combination of chitosan and gelatin. For this, first of all, plain chitosan, plain gelatin, and half by weight of chitosan and gelatin cryogels were prepared. After the scaffolds were evaluated structurally, characterization studies were carried out with composite scaffolds. The cryogels were analyzed by using chemical composition, morphology, swelling ability, and degradation behavior experiments. Then, preliminary studies on drug loading and drug release experiments were carried out by using methyl orange as a model drug. The results obtained from the study will contribute to the estimation of real drug release profiles, determine the basic physicochemical properties of a biocompatible and biodegradable material that can release drugs, and shed light on the future biological studies of the material.

2. EXPERIMENTAL SECTION

2.1. Materials

Chitosan with low molecular weight was purchased from Sigma Aldrich, USA. Gelatin (for microbiology), glutaraldehyde (25%, v/v), glacial acetic acid (100%, v/v), and methyl orange azo dye were received from Merck, Germany. Aqueous solutions and dilutions in experiments were prepared with distilled water.

2.2. Preparation of Gelatin: Chitosan Composite Cryogels

The solvent of the polymers was selected according to our previous studies as acetic acid with a volumetric ratio of 6%. To prepare the polymer solution, chitosan and gelatin were dissolved separately in an acetic acid solution and distilled water, respectively. Chitosan solution (2%, v/v) was prepared by dissolving the calculated amount of chitosan in 20 mL of 6% acetic acid solution by stirring for 24 hours. Also, the pre-determined amount of gelatin was dissolved in 20 mL of distilled water and stirred for 24 hours. Homogeneous gelatin: chitosan solution was obtained by thoroughly mixing the prepared chitosan and gelatin solutions at different volumetric ratios (100:0, 50:50, and 0:100, gelatin: chitosan). 0.5 mL of glutaraldehyde solution was added immediately to 2 mL of polymer solution and the as-prepared solution was loaded into a 2.5 plastic syringe to give cryogel a monolithic shape. The syringe was rapidly placed in cryostat and incubated at -16 °C for 3 h. At the end of the incubation time, the sample was stored for 24 h in the freezer at -16 °C. The prepared samples were thawed at room temperature and washed repeatedly with distilled water to remove the unreacted ingredients. The samples were then freeze-dried. The dried samples were stored in the refrigerator at +4 °C for further analysis.

2.3. Characterization Studies of Cryogels

Different physical, chemical, and morphological analyses were used to characterize the fabricated cryogels for further usage in drug loading and drug release studies.

Main chemical groups and, interactions between polymers and crosslinking agents were determined using Fourier Transform Infrared spectroscopy (FTIR) (PerkinElmer, FTIR/FIR/NIR Spectrometer Frontier-ATR, USA). The infrared spectra of the scaffold and polymers were measured in the wavenumber range of 4000-450 cm^{-1}.

The morphology and microstructure of cryogel were investigated using scanning electron microscopy (SEM, FE-SEM Zeiss/Supra55, Quanta 400F Field Emission, USA). The cryogel samples were prepared by coating them with a thin layer of platinum before analysis. SEM was operated at the acceleration of 5 kV and the magnification was

200x. The average pore diameter was calculated by measuring at least 50 pores of cryogel using Image-J software.

The water absorption capacity of the completely dried cryogels was determined using the gravimetric method. Dry cryogels were weighed and (a cylindrical shape with 9 mm diameter and 5 mm height, n=3) were immersed in PBS at 37 °C. At certain time intervals, the swollen cryogels were gently transferred to a filter paper to remove the excess water from the surface and weighed again. The swelling ratio of the samples was calculated according to Eq. 1;

$$SR(\%)=\left[\frac{(M_f-M_i)}{M_i}\right]\times 100 \quad \text{(Eq. 1)}$$

where Mi is the initial dry weight of the scaffold, Mf is the swollen weight of the scaffold and SR is the swelling ratio (Demir et al., 2020).

The cryogels were cut into cylindrical pieces (radius= 9 mm, height= 3 mm, n=3) and the dry weight of cryogels was recorded. After that, the samples were incubated in 20 mL centrifuge tubes filled with sterile PBS solution at 37 °C in a shaking water bath (Daihan Scientific Co. Ltd., WiseBath WB-22, Korea). At pre-determined time intervals, samples were washed with distilled water and freeze-dried. After the drying process, the weight of each sample was recorded and the weight loss percentage was calculated according to the Eq. 2;

$$DD(\%)=\left[\frac{(W_i-W_f)}{W_i}\right]\times 100 \quad \text{(Eq. 2)}$$

where Wi is the initial dry weight of the scaffold, Wf is the final dry weight of the scaffold, and DD is the degree of degradation or degradation rate (Demir et al., 2021).

2.4. Model Studies with Dye for Drug Loading and Drug Release

MO was used as the model drug to investigate the drug loading and drug release potential of the fabricated Gel:Cs cryogel scaffold, similar to the use of different dyes as model drugs in other studies previously (Demir et al., 2018; Hauck et al., 2022; Khansari et al., 2013; Pancholi et al., 2009). For the loading of the dye, the cryogel sample was immersed in 5 mL of MO solution (0.05 mg/L) at room temperature. After 48 h incubation, samples were removed from the dye solution and rinsed with a known volume of pure water. The weight of dye was analyzed by UV-Vis spectroscopy (Chebios Optimum-One UV-vis, Italy) at a wavelength of 554 nm. The dye encapsulation efficiency of each sample was calculated using Eq. 3.

$$EE,\%wt=\left[\frac{C_{dye,i}-C_{dye,w}}{C_{dye,i}}\right]\times 100 \quad \text{(Eq. 3)}$$

where EE is the encapsulation efficiency, $C_{dye,\ I}$ is the concentration of dye in the initial solution, and $C_{dye,w}$ is the concentration of dye in the washing solution.

The release of MO from the cryogels was evaluated in phosphate buffer saline (PBS at pH 7.4) solution. MO-loaded samples were immersed in plastic tubes filled with 10 mL of release medium. The tubes were incubated in a shaking water bath at 37 °C with 100 rpm. 3 mL of release medium were withdrawn at pre-determined time intervals (5, 15, 30, 60, and 240 min) and replaced with an equal volume of fresh medium. Weight of MO release was quantified by UV-Vis spectroscopy. The percentage release of the MO was calculated as cumulative using Eq.4.

Cumulative Dye Release, %wt= [(Weight of dye released)/(Weight of dye in the cryogel)]*100 (4)
The dye absorption and release experiments were done in triplicate and results are presented as mean ± SD.

3. RESULTS AND DISCUSSION

3.1. Cryogel Synthesis and Characterization

The experimental setup, cryogelation process, and typical crosslinking between gelatin and chitosan with glutaraldehyde are summarized in Figure 1. Cryogelation technique, in other words, crytropic gelation, was used in the production of scaffolds to create an interconnected macroporous structure for more effective drug absorption and release studies. In the cryogenic process, gelation occurs at subzero temperatures, leading to the formation of a polymeric network crosslinked around the icy crystals. Then, with the thawing of these crystals, an interconnected macroporous structure surrounded by highly dense polymeric walls remains. In this study, we used gelatin and chitosan as naturally derived polymers to fabricate cryogels. A general overview of the experimental setup, crosslinking mechanism, and cryogelation technique was shown in Figure 1.

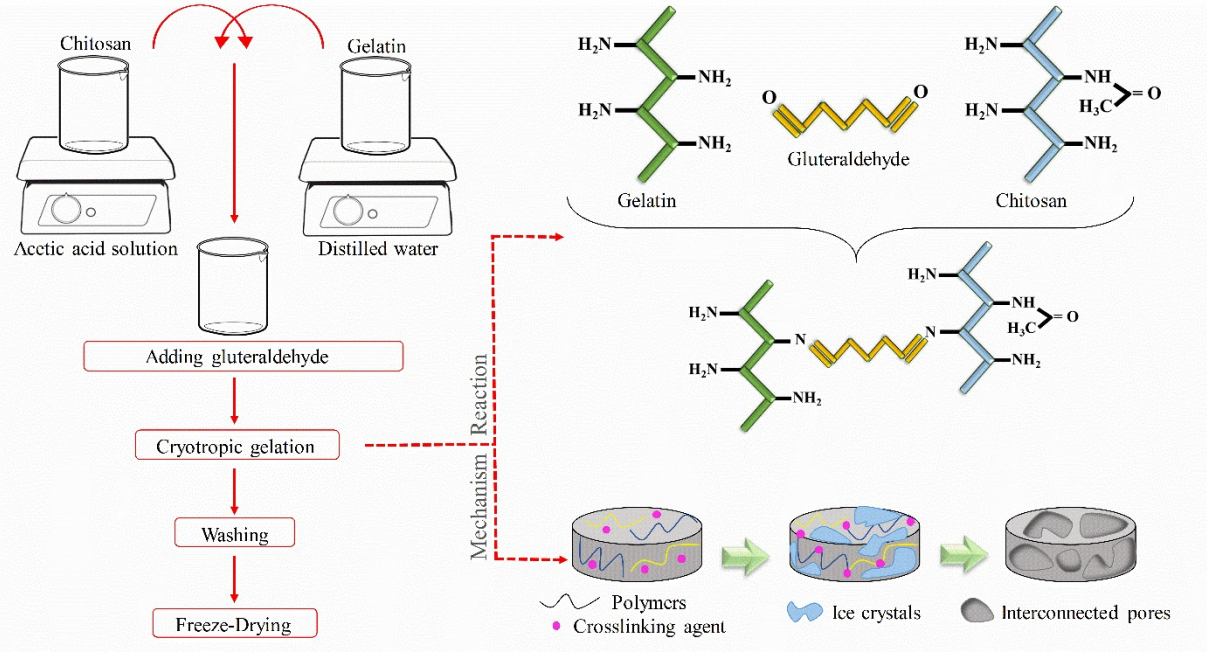

Figure 1: General overview of the experimental set-up, crosslinking mechanism, and cryogelation technique.

Before using chitosan and gelatin together, we wanted to observe the potential for scaffolding by using chitosan and gelatin separately. As the structural properties are shown in Table 1, gelatin alone exhibited a looser structure, while chitosan exhibited a more brittle and hard structure. When both polymers are used alone, materials that are not easy to apply and that are not stable enough have been produced. The composite produced with the use of chitosan and gelatin by half by weight, on the other hand, exhibited a stable, water-capable structure that could return to its original state after releasing the absorbed water. For this reason, in the continuation of the study, the composite scaffold was selected as the optimum sample.

Table 1: Effect of chitosan: gelatin ratio on the production of cryogel (Other parameters are the same).

Chitosan:Gelatin Ratio	Morphology
100:0	Fragile
50:50	Spongy
0:100	Bursting with high swelling

The chemical bond structure of the polymers used and the changes in their structures as a result of crosslinking with glutaraldehyde were analyzed with the FTIR spectra presented in Figure 2. Both polymers exhibited general characteristic bond structures before processing. For chitosan, the absorption bands around 2977 and 2888 cm^{-1} are related to C-H symmetric and asymmetric stretching, respectively. The peaks found at 1645, 1550, and 1380 cm^{-1} are attributed to Amide I (C=O stretching), Amide II (N-H bending), and Amide III (C-N stretching), respectively (Demir et al., 2016; Fernandes Queiroz et al., 2014). For gelatin, there are four major peaks located at 3230, 1631, 1524-1315, and 1240-698 cm^{-1} which correspond to Amide A, Amide I, Amide II, and Amide III regions, respectively (Pradini et al., 2018). After crosslinking the polymers in the presence of glutaraldehyde, it was observed that the intensity and positions of the peaks changed significantly. The absorption peak of the free amino group (Amide A) and OH group shifted from 3230 to 3300 cm^{-1}. The spectrum showed four strong absorption peaks at 1640, 1555, 1405, and 1068 cm^{-1} which were formed by the overlapping of the chitosan and gelatin peaks. In addition, a new absorption peak was formed at 1030 cm^{-1} which was attributed to C–O–C–O–C structure after cross-linking (Qian et al., 2011).

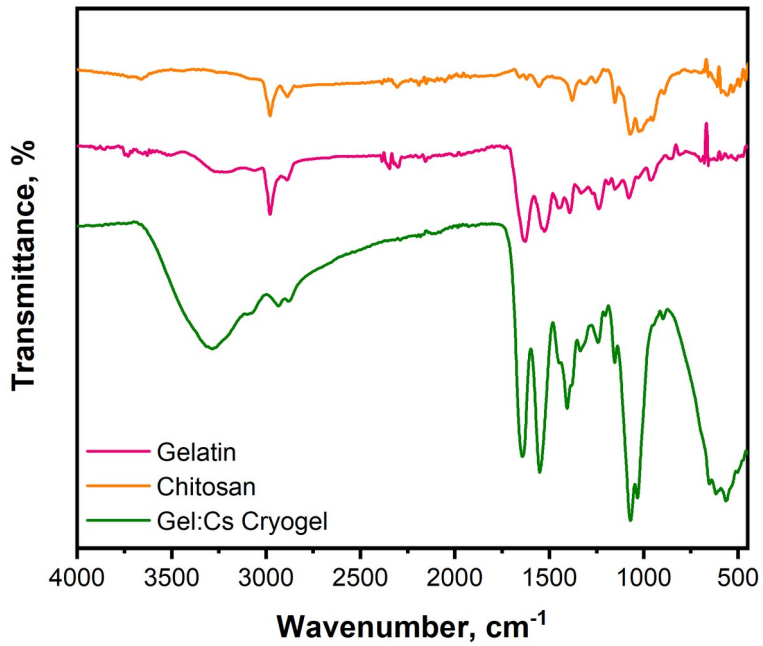

Figure 2: FTIR spectra of gelatin, chitosan, and crosslinked Gel:Cs cryogels.

To investigate the morphology of crosslinked Gel:Cs cryogel SEM images were obtained as seen in Figure 3A. The scaffold showed an interconnected porous structure as a result of the cryogelation process. In the SEM image, the gray parts represent the crosslinked polymer walls, while the dark parts show the pores. The porous structure of the material is important for cell adhesion, diffusion, migration, and proliferation in terms of tissue regeneration/new tissue formation, while it is important for drug release studies in terms of providing high drug absorption capacity and drug diffusion. In this context, it is also necessary to determine the diameter of pores. Therefore, the diameter of at least 50 pores was measured and a histogram was obtained as seen in Figure 3B. It is seen that the pore diameter range varies between 27.89 and 97.49 µm. The mean diameter was calculated at 52.95 µm. When other studies are examined, these values vary between 10-50 µm for silk cryogels (Ak et al., 2013), 15-45 µm for chitosan pectin cryogels (Demir et al., 2021) and 30-100 µm for pHEMA -poly(ethylene glycol) diacrylate-gelatin cryogels (Singh et al., 2011). In addition, the porosity of cryogel was examined gravimetrically using the ethanolic penetration method and was found as 57.05%.

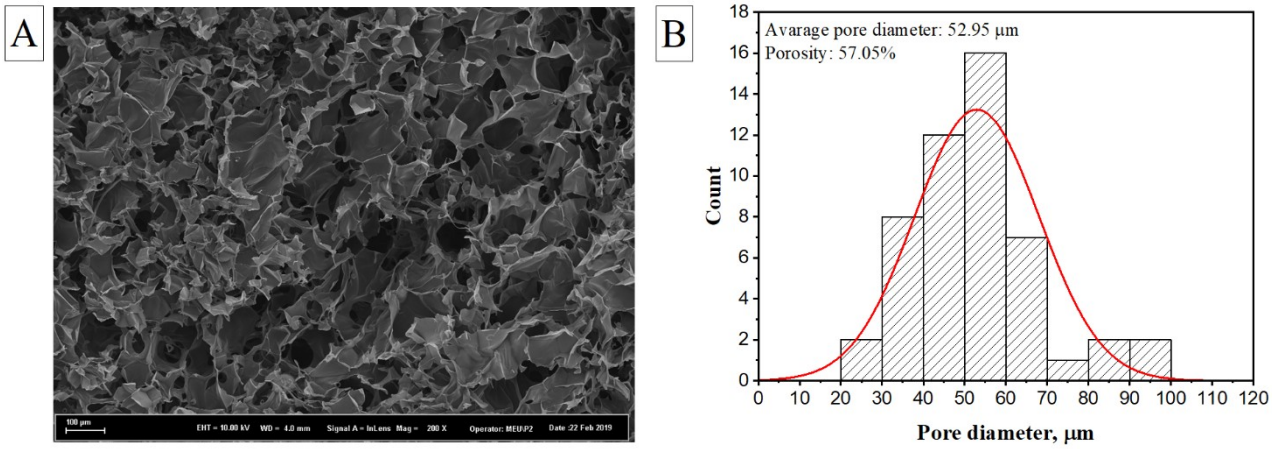

Figure 3: A) SEM image showing the porous structure of the Gel:Cs cryogels and B) Pore diameter histogram of Gel:Cs cryogel

According to the porous structure of the scaffold and the hydrophilic structure of the polymers, it was estimated that the gels can absorb high amounts of liquids. For this reason, the swelling ratios and equilibrium swelling ratios were calculated by gravimetrically measuring the change in weight of the completely dry samples after they were kept in PBS for certain periods (5,

15, 30, 60, 90, 120, 150, and 180 min). In Figure 4A, it is seen that the cryogel starts to absorb water within the first 5 minutes and reaches the equilibrium point at the end of 180 minutes. The high liquid absorption ability of the gels (approximately 500 times its own dry weight) is an important feature shows that the drug solutions can be absorbed easily into the structure of the gel scaffold. This hydrophilicity is due to the presence of carboxyl, amino, and hydroxyl groups in the polymer backbone as well as the highly porous structure of the sample (Hezaveh et al., 2012; Vo et al., 2021). When other studies are examined, it is seen that the swelling ratio values are quite high, especially for cryogels with highly interconnected macroporosity (Meena et al., 2018).

The degradation behavior of the cryogel was studied to determine whether it affects its stability and drug release behavior. For this purpose, dry gels were taken into PBS and the change in their weight was recorded for 4 weeks, and their degradation rates were monitored (Figure 4B). The sample began to degrade by 6.68±0.61% of its initial weight within the first week. Afterward, it lost 20.95±1.81% of its initial weight in 1 month. Degradation of polymeric biomaterials occurs as a result of the breaking of hydrolytic or enzymatically sensitive bonds that cause polymeric erosion. In the meantime, molecules such as drugs loaded in the polymeric system can be released into the environment depending on the degradation rate (Ghanbarzadeh & Almasi, 2013). Therefore, the drug release rate varies depending on the degradation rate of the materials. For example, in a therapy where a long duration is needed, materials with slow degradation kinetics are needed (Martins et al., 2018). Here, chitosan and gelatin, as biodegradable natural polymers, appear to exhibit faster degradation behavior than synthetic polymers, suggesting that Gel:Cs cryogel can be used as drug delivery systems for therapies with shorter durations.

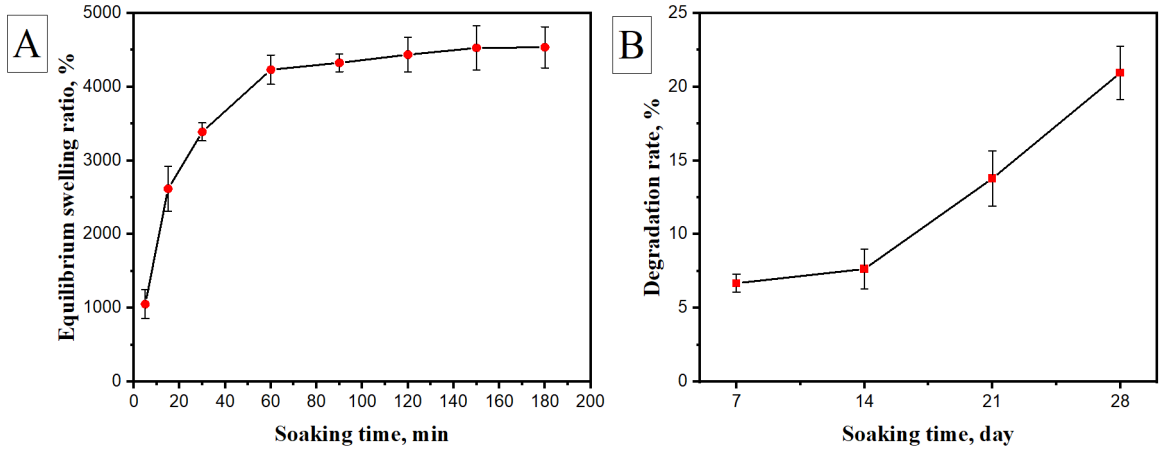

Figure 4: A) Swelling ratio versus soaking time of Gel:Cs cryogel in PBS pH 7.4 and B) Degradation rate of cryogel up to 28 days.

3.2. Dye Loading and Dye Release Behavior of Cryogels

After determining the main physicochemical properties of cryogel sample, dye loading and dye release studies were performed (Figures 5A and 4B). In these experiments, MO was used as a model drug. The cryogel samples in disc shapes were placed in an aqueous concentrated MO solution and allowed to equilibrate. It is seen that the cryogel discs absorb approximately 45% of the initial dyestuff amount after 120 minutes. In order to find the equilibrium value, the cryogels continued to hold in the dye solution and the amount of dye loaded at the end of 4 days was calculated as 50.45±4.02%. The color change in the cryogel due to the orange color of the MO before and after dye loading is also seen in the images embedded in Figure 5A. This situation can be explained by electrostatic interactions between active sites of adsorbent (Gel:Cs cryogel) and adsorbate (MO) molecules. The amine $-NH_2$ group in chitosan was able to accept a proton from a hydronium ion. As a result, electrostatic interaction easily occurred between NH_3^+ and MO^-; therefore, the cryogel showed good entrapment efficiency against MO (Loc et al., 2022). Based on the results, it can be said that Gel:Cs cryogels are suitable drug release systems for loading water-soluble, anionic, and weakly acid drug molecules such as MO.

To demonstrate the drug release behavior of MO-loaded gels, the cumulative release was monitored over time in a PBS buffer. The cumulative release of MO as a function of time is presented in Figure 5B. During the first 5 minutes of release, the cryogel provided about 3% of the MO release, while in the 90 minutes it released about 18%. The release rate reached 34.88±2.87% at the 30th minute and then slowed down and approached the equilibrium (32.94±4.01%) at the 180th minute. The rate of drug release from a polymeric system

can be affected by different events, from drug dissolution to water absorption, polymer swelling, drug dissolution through the polymer network, diffusion, and polymer erosion (Şarkaya & Allı, 2021). In our study, we can mainly relate the release during this 1 day to the rapid swelling properties of the cryogels. The high swelling capacity of the gels may have both accelerated the diffusion rate of the penetrant into the matrix and facilitated MO dissolution and diffusion of the swollen matrix through the gel layer, exhibiting a faster drug release profile up to the equilibrium swelling point of the cryogel (The cryogel reached equilibrium at a swelling rate of 4535.57±277.93% in 180 minutes, as presented in Figure 4A). The results obtained here are that a slow release occurs due to the swelling kinetics only, as a result of the strong electrostatic interactions between the MO and the polymers.

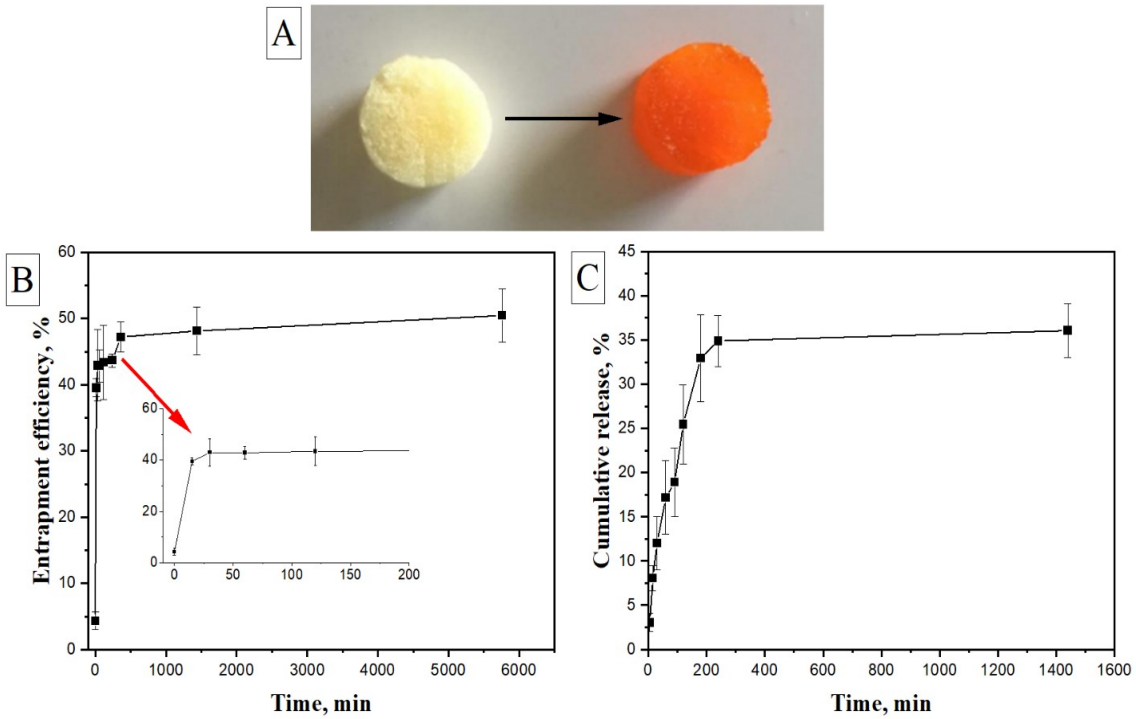

Figure 5. A) Color change in cryogel after dye adsorption, B) MO adsorption capacity versus time, and C) Time-dependent release of MO.

4. CONCLUSION

In this study, glutaraldehyde crosslinked cryogel scaffolds were fabricated, characterized, and then evaluated for drug adsorption and release studies. Considering that polymer type and the ratio is a critical production variables in cryogel production, plain chitosan, plain gelatin, and a composite scaffold combined half by weight of chitosan and gelatin were evaluated. It was observed that the composite scaffold exhibited mechanically a more stable and water-capable structure, and the study was continued with this sample. The composite cryogel showed an open network with an interconnected porous structure. The ability of cryogel as an adsorbent for MO from an aqueous dye solution was examined. In light of the experiments, the results indicate that glutaraldehyde crosslinked Gel:Cs cryogel has good characterization properties for drug loading and release applications. Using the appropriate formula and fabrication method can affect the cryogel scaffold stability and release MO, which can be targeted for drug or growth factor release for cell migration, proliferation, and formation of new tissue for future studies. This study demonstrates that we can optimize the formula of Gel:Cs cryogels and maximize the role of polymer ratio for further drug loading and release applications.

5. CONFLICT OF INTEREST

The authors have no conflict of interest.

6. REFERENCES

Ak, F., Oztoprak, Z., Karakutuk, I., & Okay, O. (2013). Macroporous Silk Fibroin Cryogels. *Biomacromolecules*, *14*(3), 719–727. https://doi.org/10.1021/bm3018033.

Ayaz, F., Demir, D., & Bölgen, N. (2021). Differential anti-inflammatory properties of chitosan-based cryogel scaffolds depending on chitosan/gelatin ratio. *Artificial Cells, Nanomedicine, and Biotechnology*, *49*(1), 682–690.

https://doi.org/10.1080/21691401.2021.2012184.

Bhasarkar, J., & Bal, D. (2019). Kinetic investigation of a controlled drug delivery system based on alginate scaffold with embedded voids. *Journal of Applied Biomaterials & Functional Materials*, *17*(2), 228080001881746. https://doi.org/10.1177/2280800018817462.

Bhat, S., Tripathi, A., & Kumar, A. (2011). Supermacroprous chitosan–agarose–gelatin cryogels: *In vitro* characterization and *in vivo* assessment for cartilage tissue engineering. *Journal of The Royal Society Interface*, *8*(57), 540–554. https://doi.org/10.1098/rsif.2010.0455.

Biondi, M., Ungaro, F., Quaglia, F., & Netti, P. A. (2008). Controlled drug delivery in tissue engineering. *Advanced Drug Delivery Reviews*, *60*(2), 229–242. https://doi.org/10.1016/j.addr.2007.08.038.

Demir, D., Ceylan, S., Göktürk, D., & Bölgen, N. (2021). Extraction of pectin from albedo of lemon peels for preparation of tissue engineering scaffolds. *Polymer Bulletin*, *78*(4), 2211–2226. https://doi.org/10.1007/s00289-020-03208-1.

Demir, D., Güreş, D., Tecim, T., Genç, R., & Bölgen, N. (2018). Magnetic nanoparticle-loaded electrospun poly(ε-caprolactone) nanofibers for drug delivery applications. *Applied Nanoscience*, *8*(6), 1461–1469. https://doi.org/10.1007/s13204-018-0830-9.

Demir, D., Öfkeli, F., Ceylan, S., & Bölgen, N. (2016). Extraction and Characterization of Chitin and Chitosan from Blue Crab and Synthesis of Chitosan Cryogel Scaffolds. *Journal of the Turkish Chemical Society, Section A: Chemistry*, *3*(3). https://doi.org/10.18596/jotcsa.00634.

Fernandes Queiroz, M., Melo, K., Sabry, D., Sassaki, G., & Rocha, H. (2014). Does the Use of Chitosan Contribute to Oxalate Kidney Stone Formation? *Marine Drugs*, *13*(1), 141–158. https://doi.org/10.3390/md13010141.

Ghanbarzadeh, B., & Almasi, H. (2013). Biodegradable Polymers. In R. Chamy (Ed.), *Biodegradation—Life of Science*. InTech. https://doi.org/10.5772/56230.

Han, H. D., Song, C. K., Park, Y. S., Noh, K. H., Kim, J. H., Hwang, T., Kim, T. W., & Shin, B. C. (2008). A chitosan hydrogel-based cancer drug delivery system exhibits synergistic antitumor effects by combining with a vaccinia viral vaccine. *International Journal of Pharmaceutics*, *350*(1–2), 27–34. https://doi.org/10.1016/j.ijpharm.2007.08.014.

Hauck, M., Dittmann, J., Zeller-Plumhoff, B., Madurawala, R., Hellmold, D., Kubelt, C., Synowitz, M., Held-Feindt, J., Adelung, R., Wulfinghoff, S., & Schütt, F. (2022). Fabrication and Modelling of a Reservoir-Based Drug Delivery System for Customizable Release. *Pharmaceutics*, *14*(4), 777. https://doi.org/10.3390/pharmaceutics14040777.

Hezaveh, H., Muhamad, I. I., Noshadi, I., Shu Fen, L., & Ngadi, N. (2012). Swelling behaviour and controlled drug release from cross-linked κ-carrageenan/NaCMC hydrogel by diffusion mechanism. *Journal of Microencapsulation*, *29*(4), 368–379. https://doi.org/10.3109/02652048.2011.651501.

Kemençe, N., & Bölgen, N. (2017). Gelatin- and hydroxyapatite-based cryogels for bone tissue engineering: Synthesis, characterization, *in vitro* and *in vivo* biocompatibility: Gelatin and hydroxyapatite cryogels for bone tissue engineering. *Journal of Tissue Engineering and Regenerative Medicine*, *11*(1), 20–33. https://doi.org/10.1002/term.1813.

Khansari, S., Duzyer, S., Sinha-Ray, S., Hockenberger, A., Yarin, A. L., & Pourdeyhimi, B. (2013). Two-Stage Desorption-Controlled Release of Fluorescent Dye and Vitamin from Solution-Blown and Electrospun Nanofiber Mats Containing Porogens. *Molecular Pharmaceutics*, *10*(12), 4509–4526. https://doi.org/10.1021/mp4003442.

Kim, Y., Dalhaimer, P., Christian, D. A., & Discher, D. E. (2005). Polymeric worm micelles as nano-carriers for drug delivery. *Nanotechnology*, *16*(7), S484–S491. https://doi.org/10.1088/0957-4484/16/7/024.

Li, J., Wang, Y., Zhang, L., Xu, Z., Dai, H., & Wu, W. (2019). Nanocellulose/Gelatin Composite Cryogels for Controlled Drug Release. *ACS Sustainable Chemistry & Engineering*, *7*(6), 6381–6389. https://doi.org/10.1021/acssuschemeng.9b00161.

Loc, N. X., Tuyen, P. T. T., Mai, L. C., & Phuong, D. T. M. (2022). Chitosan-Modified Biochar and Unmodified Biochar for Methyl Orange: Adsorption Characteristics and Mechanism

Exploration. *Toxics*, *10*(9), 500. https://doi.org/10.3390/toxics10090500.

Lu, Z., Yeh, T.-K., Tsai, M., Au, J. L.-S., & Wientjes, M. G. (2004). Paclitaxel-Loaded Gelatin Nanoparticles for Intravesical Bladder Cancer Therapy. *Clinical Cancer Research*, *10*(22), 7677–7684. https://doi.org/10.1158/1078-0432.CCR-04-1443.

Martins, J. P., Ferreira, M. P. A., Ezazi, N. Z., Hirvonen, J. T., Santos, H. A., Thrivikraman, G., França, C. M., Athirasala, A., Tahayeri, A., & Bertassoni, L. E. (2018). 3D printing: Prospects and challenges. In *Nanotechnologies in Preventive and Regenerative Medicine* (pp. 299–379). Elsevier. https://doi.org/10.1016/B978-0-323-48063-5.00004-6.

Meena, L. K., Raval, P., Kedaria, D., & Vasita, R. (2018). Study of locust bean gum reinforced cyst-chitosan and oxidized dextran based semi-IPN cryogel dressing for hemostatic application. *Bioactive Materials*, *3*(3), 370–384. https://doi.org/10.1016/j.bioactmat.2017.11.005.

Mondal, D., Griffith, M., & Venkatraman, S. S. (2016). Polycaprolactone-based biomaterials for tissue engineering and drug delivery: Current scenario and challenges. *International Journal of Polymeric Materials and Polymeric Biomaterials*, *65*(5), 255–265. https://doi.org/10.1080/00914037.2015.1103241.

Nagahama, H., Maeda, H., Kashiki, T., Jayakumar, R., Furuike, T., & Tamura, H. (2009). Preparation and characterization of novel chitosan/gelatin membranes using chitosan hydrogel. *Carbohydrate Polymers*, *76*(2), 255–260. https://doi.org/10.1016/j.carbpol.2008.10.015.

Pancholi, K., Stride, E., & Edirisinghe, M. (2009). *In Vitro* Method to Characterize Diffusion of Dye from Polymeric Particles: A Model for Drug Release. *Langmuir*, *25*(17), 10007–10013. https://doi.org/10.1021/la900694k.

Piazzini, V., Landucci, E., D'Ambrosio, M., Tiozzo Fasiolo, L., Cinci, L., Colombo, G., Pellegrini-Giampietro, D. E., Bilia, A. R., Luceri, C., & Bergonzi, M. C. (2019). Chitosan coated human serum albumin nanoparticles: A promising strategy for nose-to-brain drug delivery. *International Journal of Biological Macromolecules*, *129*, 267–280. https://doi.org/10.1016/j.ijbiomac.2019.02.005.

Pradini, D., Juwono, H., Madurani, K. A., & Kurniawan, F. (2018). A preliminary study of identification halal gelatin using quartz crystal microbalance (QCM) sensor. *Malaysian Journal of Fundamental and Applied Sciences*, *14*(3), 325–330.

Qian, Y.-F., Zhang, K.-H., Chen, F., Ke, Q.-F., & Mo, X.-M. (2011). Cross-Linking of Gelatin and Chitosan Complex Nanofibers for Tissue-Engineering Scaffolds. *Journal of Biomaterials Science, Polymer Edition*, *22*(8), 1099–1113. https://doi.org/10.1163/092050610X499447.

Rogers, Z. J., & Bencherif, S. A. (2019). Cryogelation and Cryogels. *Gels*, *5*(4), 46. https://doi.org/10.3390/gels5040046.

Şarkaya, K., & Allı, A. (2021). Synthesis and characterization of cryogels of p(HEMA-N-vinylformamide) and p(HEMA-N-Vinylpyrrolidone) for chemical release behaviour. *Journal of Porous Materials*, *28*(3), 853–865. https://doi.org/10.1007/s10934-021-01037-9.

Shera, S. S., Sahu, S., & Banik, R. M. (2018). Preparation of Drug Eluting Natural Composite Scaffold Using Response Surface Methodology and Artificial Neural Network Approach. *Tissue Engineering and Regenerative Medicine*, *15*(2), 131–143. https://doi.org/10.1007/s13770-017-0100-z.

Singh, D., Tripathi, A., Nayak, V., & Kumar, A. (2011). Proliferation of Chondrocytes on a 3-D Modelled Macroporous Poly(Hydroxyethyl Methacrylate)–Gelatin Cryogel. *Journal of Biomaterials Science, Polymer Edition*, *22*(13), 1733–1751. https://doi.org/10.1163/092050610X522486.

Surya, R., Mullassery, M. D., Fernandez, N. B., Thomas, D., & Jayaram, P. S. (2020). Synthesis and characterization of a pH responsive and mucoadhesive drug delivery system for the controlled release application of anti-cancerous drug. *Arabian Journal of Chemistry*, *13*(5), 5262–5276. https://doi.org/10.1016/j.arabjc.2020.03.005.

Vo, T. S., Vo, T. T. B. C., Nguyen, T. S., & TiEn, T. T. (2021). Fabrication and Characterization of Gelatin/Chitosan Hydrogel Utilizing as Membranes. *Journal of the Turkish Chemical Society Section A: Chemistry*, 1045–1056. https://doi.org/10.18596/jotcsa.942478.

Wang, J., Wang, G., Shan, H., Wang, X., Wang, C., Zhuang, X., Ding, J., & Chen, X. (2019).

Gradiently degraded electrospun polyester scaffolds with cytostatic for urothelial carcinoma therapy. *Biomaterials Science*, *7*(3), 963–974. https://doi.org/10.1039/C8BM01317A.

Yao, J., Wang, Y., Ma, W., Dong, W., Zhang, M., & Sun, D. (2019). Dual-Drug-Loaded Silk Fibroin/PLGA Scaffolds for Potential Bone Regeneration Applications. *Journal of Nanomaterials*, *2019*, 1–16. https://doi.org/10.1155/2019/8050413.

Yusop, A. H., Sarian, M. N., Januddi, F. S., Ahmed, Q. U., Kadir, M. R., Hartanto, D., Hermawan, H., & Nur, H. (2018). Structure, degradation, drug release and mechanical properties relationships of iron-based drug eluting scaffolds: The effects of PLGA. *Materials & Design*, *160*, 203–217. https://doi.org/10.1016/j.matdes.2018.09.019.